Quantum Molecular Collision Theory with Problems based on Matlab

Millard H. Alexander

CONTENTS

I. INTRODUCTION

In these lectures, I will present an Introduction to some key concepts and ideas in the quantum description of molecular collisions. Working through these topics, and the associated problems, will give you the background to embark on a research career in theoretical chemistry

II. ONE-DIMENSIONAL SCATTERING BY A BARRIER

A. Rectangular Barrier

Consider one-dimensional scattering by a rectangular barrier, illustrated here

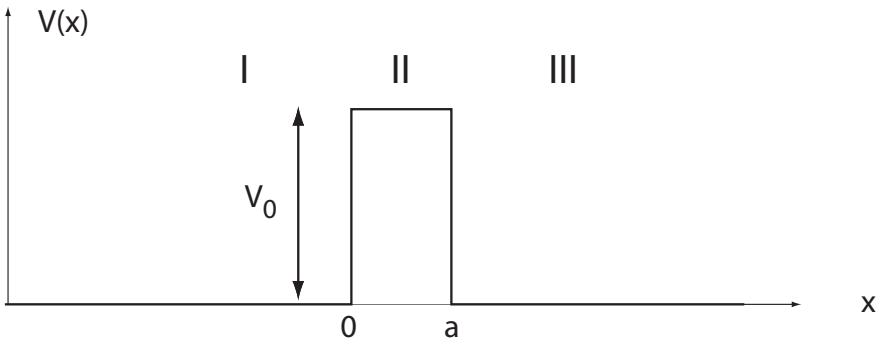

FIG. 1. A one-dimensional rectangular barrier of height V_0 and width a.

Since the potential is constant (and equal to zero) in region I, the wavefunction, which is a solution to the one-dimensional, time-independent Schrodinger equation

$$H\psi = [KE_{op} + V(x)] = \left[-\frac{\hbar^2}{2m}\frac{d^2}{dx^2} + V(x)\right]\psi = E\psi$$

can be written as

$$\psi_I = e^{ikx} + Re^{-ikx} \tag{1}$$

where the wavevector is defined as $k = (2mE/\hbar^2)^{1/2}$. This corresponds to an incoming wave propagating to the right and a reflected wave, with amplitude R. In region III the wavefunction can be written as

$$\psi_{III} = Se^{ikx} \tag{2}$$

which corresponds to a scattered wave with amplitude S. Obviously $|S|^2 + |R|^2 = 1$, since flux has to be conserved. In region II, the form of the wavefunction depends on whether the energy is greater than or less than V_0. In the former case, which corresponds to the classically allowed situation, we have

$$\psi_{II} = Ae^{ik'x} + Be^{-ik'x} \tag{3}$$

where $k' = [2m(E - V_0)/\hbar^2]^{1/2}$. When $E < V_0$, the form of the wavefunction is

$$\psi_{II} = Ae^{\kappa x} + Be^{-\kappa x} \tag{4}$$

where $\kappa = [2m(V_0 - E)/\hbar^2]^{1/2}$

The wavefunction and its first derivative must be continuous as the boundaries between regions I and II and between regions II and III. These two continuity conditions will allow us to eliminate A and B, and obtain an expression of S and R. To do so we proceed as follows:

At $x = 0$, the boundary between regions I and II, the value of ψ_I and its first derivative can be expressed in matrix notation as

$$\begin{bmatrix} \psi_I(x=0) \\ \psi_I'(x=0) \end{bmatrix} = \begin{bmatrix} 1 & 1 \\ ik & -ik \end{bmatrix} \begin{bmatrix} 1 \\ R \end{bmatrix} = \mathbf{M}_L \begin{bmatrix} 1 \\ R \end{bmatrix} \tag{5}$$

Similarly, at $x = 0$ the the value of ψ_{II} and its first derivative can be expressed in matrix notation as

$$\begin{bmatrix} \psi_{II}(x=0) \\ \psi_{II}'(x=0) \end{bmatrix} = \begin{bmatrix} 1 & 1 \\ ik' & -ik' \end{bmatrix} \begin{bmatrix} A \\ B \end{bmatrix} = \mathbf{M}_R \begin{bmatrix} A \\ B \end{bmatrix} \tag{6}$$

Note that when $E < V_0$, the matrix $\mathbf{M}_R$ is

$$\mathbf{M}_R = \begin{bmatrix} 1 & 1 \\ \kappa & -\kappa \end{bmatrix} \tag{7}$$

Setting Eqs. (5) and (6) equal (which is the continuity condition on the function and its first derivative) we obtain

$$\begin{bmatrix} A \\ B \end{bmatrix} = \mathbf{M}_R^{-1} \mathbf{M}_L \begin{bmatrix} 1 \\ R \end{bmatrix} \tag{8}$$

Now, at $x = a$, the wavefunction in region II and its first derivative can be expressed as

$$\begin{bmatrix} \psi_{II}(x=a) \\ \psi_{II}'(x=a) \end{bmatrix} = \begin{bmatrix} e^{ik'a} & e^{-ik'a} \\ ik'e^{ik'a} & -ik'e^{-ik'a} \end{bmatrix} \begin{bmatrix} A \\ B \end{bmatrix} = \tilde{\mathbf{M}} \begin{bmatrix} A \\ B \end{bmatrix} \tag{9}$$

When $E < V_0$, the matrix $\tilde{\mathbf{M}}$ is

$$\tilde{\mathbf{M}} = \begin{bmatrix} e^{\kappa a} & e^{-\kappa a} \\ \kappa e^{\kappa a} & -\kappa e^{-\kappa a} \end{bmatrix} \tag{10}$$

Also, at $x = a$ the wavefunction in region III and its first derivative can be written as

$$\begin{bmatrix} \psi_{III}(x=a) \\ \psi'_{III}(x=a) \end{bmatrix} = S \begin{bmatrix} e^{ika} \\ ike^{ika} \end{bmatrix} \tag{11}$$

Now, inserting Eq. (8) into Eq. (9) and equating Eqs. (9) and (10) (the continuity condition at $x = a$) gives

$$\begin{bmatrix} Se^{ika} \\ ikSe^{ika} \end{bmatrix} = \tilde{\mathbf{M}}\mathbf{M}_R^{-1}\mathbf{M}_L \begin{bmatrix} 1 \\ R \end{bmatrix} = \mathbf{M} \begin{bmatrix} 1 \\ R \end{bmatrix} \tag{12}$$

Equation (12) is equivalent to solving the following set of linear equations for S and R, namely

$$\begin{bmatrix} -e^{ika} & M_{12} \\ -ike^{ika} & M_{22} \end{bmatrix} \begin{bmatrix} S \\ R \end{bmatrix} = \begin{bmatrix} -M_{11} \\ -M_{21} \end{bmatrix} \tag{13}$$

Problem 1

Write a Matlab script to determine the coefficients S and R as a function of the energy. Use atomic units ($\hbar = 1$), with $m = 1822$ (the mass of the H atom in atomic units), $V_0 = 8 \times 10^{-4}$, and $a = 3a_0$. Matrices can be defined easily in Matlab, for example, once you have given a value to k', `mtilde = [ exp(i*k*a) exp(-i*k*a) ; i*k*exp(i*k*a) -i*k*exp(-i*k*a)];`

The inverse of matrix `mat` is given by `inv(mat)`. The solution of a set of linear equations

$$\mathbf{M}\,\mathbf{c} = \mathbf{r}$$

where $\mathbf{M}$ is a square matrix and $\mathbf{c}$ and $\mathbf{r}$ are column vectors, is given by

`c = M \ r`.

Hint: To help you debug your Matlab script, Tab. I lists some values of $|S|^2$ and $|R|^2$ for several energies

TABLE I. Square of the scattering and reflection coefficients for scattering by a rectangular barrier. $V_0 = 8 \times 10^{-4}$, $a = 3$, $m = 1822$.

E	$\|R\|^2$	$\|S\|^2$
4.10e–4	9.9688e–1	3.1240e–3
8.10e–4	8.5295e–1	1.4705e–1
1.21e–3	7.5028e–2	9.2497e–1
1.61e–3	9.1131e–2	9.0887e–1
2.01e–3	1.7417e–5	9.9998e–1

Problem 2

A plot of the correct values should show that $|R|^2$ goes nearly to zero at the energies 3.0094e-4, 1.2038e-3, and 2.7085e-3. In other words, at these energies there is no reflection. The collision of the incoming wave proceeds as if there is no barrier at all. Why is this?

Problem 3

Finally, for a large mass (m=50*1822), at very low energy (e=1×10^{-5} hartree), the square of the scattering amplitude $|S|^2$ becomes larger than one. This is physically impossible. Why does this result occur?

B. General Potential: Time-independent treatment

Suppose we have an arbitrary potential $V(x)$ which goes to zero as $x \to \pm\infty$. At $x = -\infty$, we designate the two linearly independent solution of the Schrodinger equation as

$$\lim_{x\to-\infty} \psi^{(+)}(x) = e^{ikx} \tag{14}$$

and

$$\lim_{x\to-\infty} \psi^{(-)}(x) = e^{-ikx} \tag{15}$$

To obtain $\psi^{(\pm)}$ at all values of x, we can use the Numerov method.[1] We define an equispaced grid with points $x_0, x_1, x_2, ..., x_n$ with spacing h. The values of $\psi^{(\pm)}$ at the grid points are given by the 3-term recursion relation.

$$\left(1+\frac{h^2}{12}k_{n+1}^2\right)\psi_{n+1}^{(\pm)} = \left(2-\frac{10h^2}{12}k_n^2\right)\psi_n^{(\pm)} - \left(1+\frac{h^2}{12}k_{n-1}^2\right)\psi_{n-1}^{(\pm)} \tag{16}$$

where

$$k_n^2 = k_n^2(x_n) = 2m\left[E - V(x_n)\right]/\hbar^2$$

Procedurally, one starts with values of $\psi^{(\pm)}$ at x_1 and x_2 and then uses Eq. (16) to obtain $\psi^{(\pm)}(x = x_3)$ and so on, until one has propagated the solution to $x = x_n$. Because the potential is real (presumably) the Hamiltonian is invariant with respect to complex conjugation, so

$$\psi^{(-1)}(x) = \psi^{(-1)}(x)^* \tag{17}$$

Thus we need only propagate one of the linearly independent solutions.

At large x, where the potential has again gone to zero,

$$\lim_{x\to\infty}\psi^{(+)}(x) = Ae^{ikx} + Be^{-ikx} \tag{18}$$

and, because of Eq. (17),

$$\lim_{x\to\infty}\psi^{(-)}(x) = B^*e^{ikx} + A^*e^{-ikx} \tag{19}$$

We can obtain the coefficients A and B by fitting $\psi^{(+)}(x_{n-1})$ and $\psi^{(+)}(x_n)$, namely

$$\begin{bmatrix} \exp(ikx_{n-1}) & \exp(-ikx_{n-1}) \\ \exp(ikx_n) & \exp(-ikx_n) \end{bmatrix} \begin{bmatrix} A \\ B \end{bmatrix} = \begin{bmatrix} \psi^{(+)}(x_{n-1}) \\ \psi^{(+)}(x_n) \end{bmatrix} \tag{20}$$

At this point we wish to impose the scattering boundary conditions [Eqs. (1) and (2)]. In particular, at large x we want the wavefunction to correspond to purely outgoing boundary conditions, for $x \to -\infty$ we want the wavefunction to behave as $\lim_{x\to-\infty}\psi(x) = \psi^{(+)}(x) + R\psi^{(-)}(x)$. The large x condition can be imposed by multiplying $\psi^{-1}(x)$ by a constant C so

that

$$\lim_{x\to\infty}\left[\psi^{(+)}(x)+C\psi^{(-)}(x)\right]=Se^{ikx}$$

From Eqs. (18) and (19) we see that this can be achieved if

$$C=-B/A^*$$

so that

$$\lim_{x\to\infty}\left[\psi^{(+)}(x)+C\psi^{(-)}(x)\right]=\left(A-\frac{BB^*}{A^*}\right)e^{ikx}$$

Thus,

$$S=A-\frac{|B^2|}{A^*}$$

Similarly, we can use Eqs. (14) and (15) to show that

$$\lim_{x\to-\infty}\left[\psi^{(+)}(x)+C\psi^{(-)}(x)\right]=e^{ikx}+Ce^{-ikx}=e^{ikx}-\frac{B}{A^*}e^{-ikx}$$

Thus, the reflection amplitude is

$$R=-\frac{B}{A^*}.$$

Problem 4

Plot the dependence on x of the Eckhart barrier (which is a model for chemical reaction dynamics), namely

$$V(x)=V_0\,\mathrm{sech}(ax)^2$$

with $V_0=3\times10^{-4}$, $a=3a_0$ and where

$$\mathrm{sech}(ax)=\frac{1}{\cosh(ax)}=\frac{2}{e^{ax}+e^{-ax}}$$

Problem 5

Modify your Matlab script from subsection A to obtain the scattering and reflection amplitude for scattering by an Eckhart barrier with $m = 1822$, V_0=8e-4, and $a = 3$. Plot the resulting values of $|S|^2$ and $|R|^2$ and compare these with the rectangular barrier of subsection A. Hint: to check that your script is working, you could propagate to all x the wavefunctions which have at $r \to -\infty$ the asymptotic for given in Eqs. (14) and (15). These two solutions should be complex conjugates of each other. To make sure you have the code working properly, Tab. II gives the answers at two energies.

TABLE II. Square of the scattering and reflection coefficients for scattering by an Eckart barrier. $V_0 = 8 \times 10^{-4}$, $a = 1$, $m = 1822$.

E	R	S	$\|R\|^2$	$\|S\|^2$
1.70e–4	–2.9080e–1 + 9.5425e–1 i	–6.6528e–2 – 2.0274e–2 i	9.9516e–1	4.8370e–3
1.17e–3	–2.4765e–1 + 2.6432e–2 i	–1.0242e–1 – 9.6306e–1 i	6.2030e–2	9.3797e–1

III. ELASTIC SCATTERING IN THREE DIMENSIONS: CLASSICAL TREATMENT

A. Separation of center-of-mass motion

See the handout I am distributing, taken from the book by McDaniel.[2]

B. Scattering in the center-of-mass frame

Now that we have separated out the motion of the center-of-mass, we need consider only the scattering of a particle of mass μ by a potential $V(r)$. More details on this classical treatment can be found in a number of places.[3]

Since the potential depends only on the distance, the angular momentum l is conserved, namely

$$l = \mu r^2 \dot{\theta} = const \tag{21}$$

where the superscript "dot" indicates differentiation with respect to time. (Note that this equation is the statement of Kepler's law – equal angles are swept out in equal time – since $d\theta/dt$ is constant). Also, since, in general,

$$\vec{l} = \vec{r} \times \vec{p} = \vec{r} \times m\vec{v} = mvr\sin(\theta) = mvb\,,$$

where b is the impact parameter. This is illustrated in Fig. 12. Since $\vec{v}$ lies along the z axis, we see from Fig. 12 that l is perpendicular to the scattering plane with magnitude mvb.

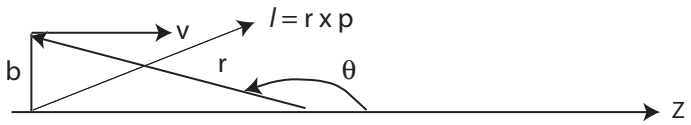

FIG. 2. Scattering of an effective particle of mass μ. Initially, the system is described by the impact parameter b and the velocity v. The angular momentum $\vec{l}$ is perpendicular to the scattering plane and here points, for this choice of $\vec{v}$ and b, into the plane.

Now, the total energy is the sum of the kinetic and potential energy

$$E = \frac{1}{2}\mu\dot{r}^2 + \frac{1}{2}\mu r^2\dot{\theta}^2 + V(r) = \frac{1}{2}\mu\dot{r}^2 + \frac{l^2}{2\mu r^2} + V(r) \tag{22}$$

Asymptotically, at large r, where the potential vanishes, the energy is purely kinetic, so that the asymptotic velocity is given by

$$\lim_{r\to\pm\infty}\dot{r} \equiv v = \left(\frac{2E}{\mu}\right)^{1/2}$$

so that

$$\frac{l^2}{2\mu} = \frac{(\mu v b)^2}{2\mu} = Eb^2 \tag{23}$$

This allows us to rewrite Eq. (22) as

$$E = \frac{1}{2}\mu\dot{r}^2 + E\frac{b^2}{r^2} + V(r) \tag{24}$$

We can solve this equation for $\dot{r}$, obtaining

$$\dot{r} = \pm \left\{ \frac{2E}{\mu} \left[1 - \frac{b^2}{r^2} - \frac{V(r)}{E} \right] \right\}^{1/2} \tag{25}$$

Before the collision, at large separation, $V(r)$ is zero so that $\dot{r} = -v = -(2E/\mu)^{1/2}$. The particles are approaching so that r is decreasing, thus $\dot{r}$ is negative. The velocity decreases until the particles reach their distance of closest approach. At this point $\dot{r} = 0$, The value of r where this occurs defines the *turning point*, r_{min}. Mathematically, this is the value of r for which

$$\left[1 - \frac{b^2}{r^2} - \frac{V(r)}{E} \right] = 0$$

For head-on collisions (zero impact parameter) the turning point occurs where $V(r) = E$, at which point all the energy is potential energy. As b increases, the turning point will increase.

Problem 6

Consider the interaction between two argon atoms, which can be well described by a Morse potential

$$V(r) = D_e \left\{ \exp\left[-2\beta(r - r_e)\right] - 2\exp\left[-\beta(r - r_e)\right] \right\}$$

with, in atomic units $r_e = 7.1053$, $\beta = 0.89305$, and $D_e = 4.456 \times 10^{-4}$.

Write a Matlab function script to determine the value of $V(r)$ for an arbitrary r. Call this script, say, `vmorse(r)`. Then, write a function script to determine the value of

$$\left[1 - \frac{b^2}{r^2} - \frac{V(r)}{E} \right].$$

Call this function, say, `term(r)`, which will be a function only of r. The values of b and E must also be available to the function script. This can be done by making the variables b and E "global" (see the Matlab help). This is done by inserting the statement

```
global E b
```

in both your calling script (or the command window) *and* in the function script.

Once both `vmorse(r)` and `term(r)` are debugged, then you can determine the turning point by using the Matlab command

`rmin=fzero('term',xx)`

Here `xx` is an initial numerical guess for the turning point (a good starting point is $xx = 5$). Assume that $E = 0.006$ and use, in an initial check b=0. Check that everything is working by then calculating the value of

$$\left[1 - \frac{b^2}{r^2} - \frac{V(r)}{E}\right]$$

at the turning point, namely

`rmin=fzero('term',xx); term(rmin)`

You'll sometimes find (depending on E and b) that `fzero` will give you a turning point for which the term in square brackets is negative, so that you're slightly inside the true turning point. To correct for this, add a small number to the turning point, in other words, define the turning point as

`rmin=fzero('term',xx)+1.e-12`

Now, plot the turning point as a function of impact parameter for $E = 0.006$.

After the particle has reached the turning point then r will increase (out to infinity) so that $\dot{r}$ is positive.

Now we can use the chain rule to write

$$\frac{d\theta}{dr} = \frac{d\theta}{dt}\frac{dt}{dr} = \frac{\dot{\theta}}{\dot{r}}$$

so that

$$d\theta = \frac{\dot{\theta}}{\dot{r}}dr =$$

We can now use Eqs. (21) and (23) to write

$$d\theta = \left(\frac{2E}{\mu}\right)^{1/2}\frac{b}{r^2\dot{r}}dr$$

If we now introduce Eq. (25) we obtain

$$d\theta = \pm\frac{b}{r^2}\left[1 - \frac{b^2}{r^2} - \frac{V(r)}{E}\right]^{-1/2} dr \tag{26}$$

This can be integrated to give

$$\theta = \theta_0 \pm b\int_{\infty}^{r_{min}} r^{-2}\left[1 - \frac{b^2}{r^2} - \frac{V(r)}{E}\right]^{-1/2} dr \tag{27}$$

If the initial direction of motion defines the z axis, then, asymptotically the particle starts at $-\infty$ so that $\theta_0 = \pi$ (see Fig. 12) The angle defined by $\vec{r}\cdot\hat{z}$ decreases as the collision occurs. For a head-on collision, where b=0, the deflection angle is $+\pi$. Although the integrand is a positive number, the integral itself, taken from a large value of r to a small value, will be negative. Thus, we need to take the positive sign. After the collision the angle still decreases as the particle moves from the classical turning point out to $+\infty$. The amount the angle of deflection changes after reaching to turning point is identical to the amount the angle of deflection changes before reaching the turning point. Thus, finally, after the collision, the angle of deflection is given by

$$\theta = \pi + 2b\int_{\infty}^{r_{min}} r^{-2}\left[1 - \frac{b^2}{r^2} - \frac{V(r)}{E}\right]^{-1/2} dr \tag{28}$$

Reversing the order of integration to be the normal positive sense where the lower limit of integration is less than the upper limit, we have

$$\theta = \pi - 2b\int_{r_{min}}^{\infty} r^{-2}\left[1 - \frac{b^2}{r^2} - \frac{V(r)}{E}\right]^{-1/2} dr \tag{29}$$

Problem 7

For the simple case of hard sphere scattering, the potential is defined by

$$V(r) = 0,\ r > \sigma\ \text{, and } V(r) = +\infty,\ r \leq \sigma$$

In this case the turning point is $r_{min} = \sigma$ for $b \leq \sigma$. Note that the deflection angle does

not depend on E.

For $b > \sigma$ there is no scattering. The incident particle moves in a straight line so that after the collision $\theta = 0$.

The range of integration in Eq. (29) is $r = \sigma$ to $r = \infty$. Show that if you let $b = x\sigma$, where $x \leq 1$ and $r = \rho\sigma$, then the expression for $\theta_{hs}(b)$ is

$$\theta_{hs}(b) = \pi - 2x \int_1^\infty \frac{d\rho}{\rho(\rho^2 - x^2)^{1/2}}$$

Then use the Wolfram online integrator [4] to obtain a simple closed-form expression for the hard-sphere deflection angle as a function of $x = b/\sigma$.

Then, plot $\theta(b)$ for the hard sphere. To check yourself, what should be the value for $b = 0$ and for $b = \sigma$?

Problem 8

For the scattering of two Ar atoms, write a Matlab script to determine the deflection angle as a function of b. To do so, first write a function script `integrand` which evaluates (similarly to your function script `term`)

$$r^{-2}\left[1 - \frac{b^2}{r^2} - \frac{V(r)}{E}\right]^{-1/2}$$

Again, the function should be just of the variable r, with the values of b and E transferred by a `global` statement.

Then, evaluate the integral using Matlab's numerical quadrature function `quad('integrand',rmin,3000)`, where `rmin` is the turning point (determined by the procedure you previously used) and the lower limit of integration is set to a large negative number (perhaps 3000 is too large, you should experiment).

Finally, plot $\theta(b)$ for the collision of two Ar atoms at $E = 0.006$. Compare this to the hard-sphere deflection angle. You can assume the the hard-sphere radius σ is equal to the value for which $V(r) = E$ when $E = 0.006$.

Although Matlab runs very fast, the procedure outlined above is quite inefficient. Even after $V(r)$ goes to zero, the integral in Eq. (29) is slow to converge.[5] A more efficient procedure would be to rewrite this equation as

$$\theta = \pi - 2b\left[\int_{r_{min}}^{R} r^{-2}\left[1 - \frac{b^2}{r^2} - \frac{V(r)}{E}\right]^{-1/2} dr + \int_{R}^{\infty} r^{-2}\left[1 - \frac{b^2}{r^2}\right]^{-1/2} dr\right] \tag{30}$$

where R is a value large enough that $V(R) \cong 0$ (I think $R = 20$ will be sufficient in the case of Ar–Ar collisions). The equation for $\theta(b)$ can be rewritten as

$$\theta = \pi - 2b\left[\int_{r_{min}}^{R} r^{-2}\left[1 - \frac{b^2}{r^2} - \frac{V(r)}{E}\right]^{-1/2} dr + \int_{R}^{\infty} \frac{dr}{r\left[r^2 - b^2\right]^{1/2}}\right] \tag{31}$$

The 2^{nd} integral can be evaluated analytically (you have already done so for the hard-sphere example). See if you can implement this addition to come up with a more efficient determination of $\theta(b)$.

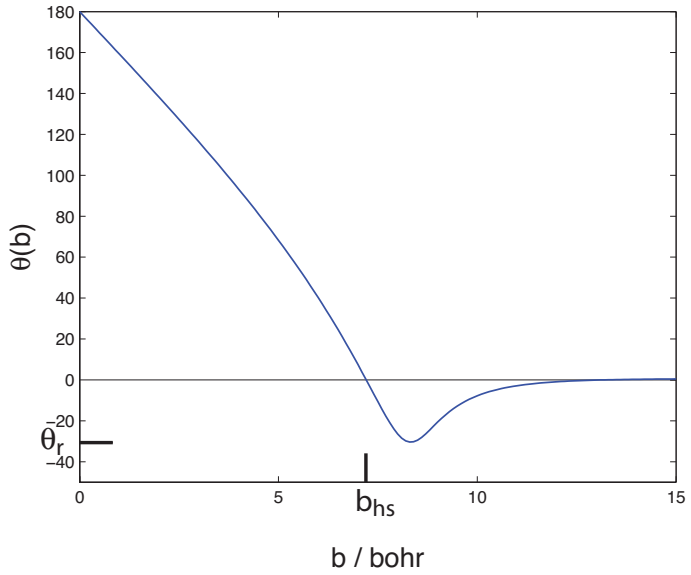

FIG. 3. Deflection function for Ar–Ar scattering, $E = 0.002$.

Figure 3 shows the dependence on b for the Ar–Ar deflection function at $E = 0.002$. For head-on scattering ($b = 0$) the deflection is 180^o. As the impact parameter decreases,

so does the deflection angle. Eventually, the deflection is zero. The point at which this occurs is called the hard-sphere impact parameter. At larger values of b, the scattering is dominated by the attractive part of the potential, so that the particle is pulled in by the potential and eventually scatters out to the other side of the z axis. This corresponds to a negative deflection angle. This negative (attractive) scattering reaches a maximum, at an angle called the *rainbow* angle (the name comes because of an analogy with the scattering of light by rain droplets). At larger impact parameter the deflection angles goes gradually to zero. Eventually, at very large b, the particle moves on by in a straight line, not sensing the potential at all.

C. Classical differential cross section

Still in the center-of-mass frame, consider a beam of particles with mass μ incident from $r = -\infty$. Any particle coming in at impact parameter b will be scattered out at a polar angle $\theta(b)$. Because the potential depends only on r, the scattering will be cylindrically symmetric. Thus, any particle which approaches the target through a circular ring of radius b will be scattered out through a spherical annulus with polar angle θ (this is the ring on the surface of a sphere with polar angle θ and all values of the azimuthal angle ϕ). This is shown in the next figure

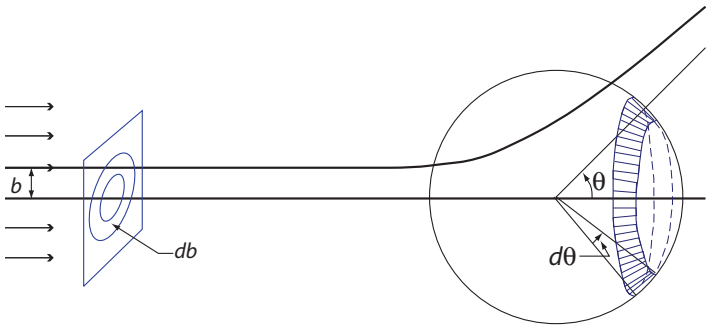

FIG. 4. Scattering of an incident beam of particles by a center of force (taken from fig. 3.1 of H. Goldstein, *Classical Mechanics*).

We shall designate by I the total number of particles per unit time approaching the target. The flux of particles (number per unit time per unit area) approaching through the cylindrical ring of radius b is $J_i = I/(2\pi b db)$. The flux of particles then emerging through the spherical annulus corresponding to polar angle θ (designated Θ in Fig. 4) is

$J_s = I/[2\pi \sin(\theta) d\theta]$. Note that J_s has units of number per unit time per unit solid angle. The ratio of the scattered flux per unit solid angle to the incoming flux per unit area is called the *differential cross section*

$$\sigma(\theta) = \frac{J_s}{J_i} = \frac{bdb}{\sin(\theta)d\theta} = \left| \frac{b}{\sin(\theta)d\theta/db} \right| , \tag{32}$$

which has units of area (hence a *cross section*). We introduce the absolute value sign, since the derivative can be both positive or negative. The differential cross section is sometimes called $d\sigma(\theta)$, $d\sigma/d\theta$, or $d\sigma/d\Omega$.

In the laboratory, it is impossible (or very difficult) to specify the location of the particle around the circle of radius b in Fig. 4, so that all possible impact parameters around this circle are sampled. Consequently, it is impossible to measure the sign of the deflection angle, in other words, impossible to distinguish particles which are scattered through angle $+\theta$ from those that are scattered through angle $-\theta$. An experiment measures the scattering at angle θ arising from both the repulsive branch of the potential, scattering at a positive deflection and the attractive branch of the potential scattering at a negative deflection. Thus, for any angle θ less than the rainbow angle, there will be three contributions to the differential cross section: one from the repulsive scattering at positive deflection angle and two from attractive scattering with negative deflection angle. This is shown in Fig. 5

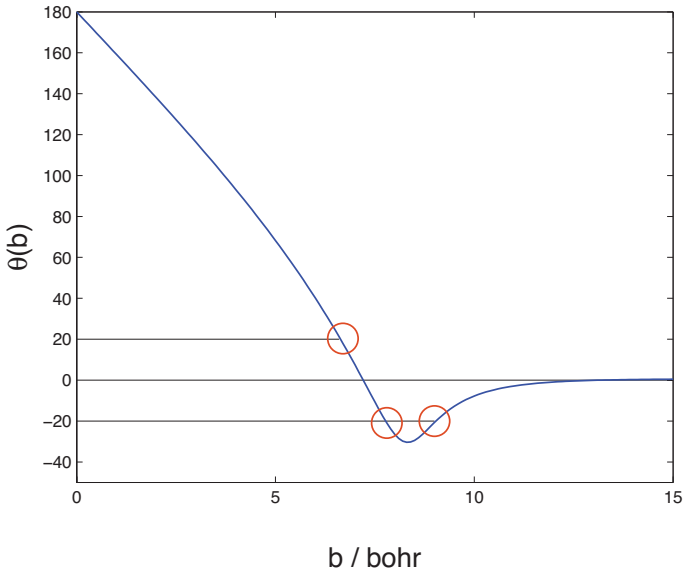

FIG. 5. Three different impact parameters will contribute to scattering at 20^o.

For angles greater than the rainbow angle, only the repulsive branch will contribute. Since the derivative of the deflection function appears in the denominator of the expression for the differential cross section [Eq. (32)], the largest differential cross sections will occur for angles at which $\theta(b)$ is nearly flat: namely at small deflection angles (forward scattering) and in the region of the rainbow. Large differential cross sections imply that incoming flux associated with many impact parameters will all appear at a single (or small range of) scattering angles.

Figure 6 shows the classical differential cross section (multiplied by $\sin(\theta)$) for Ar–Ar scattering at an energy of 0.002 Hartree. As we will see in the next section, the quantum treatment will smooth out the classical singularities at $\theta = 0$ and $\theta = \theta_R$. This will give rise to quantum interference (just like in the classic two-slit experiment [6]).

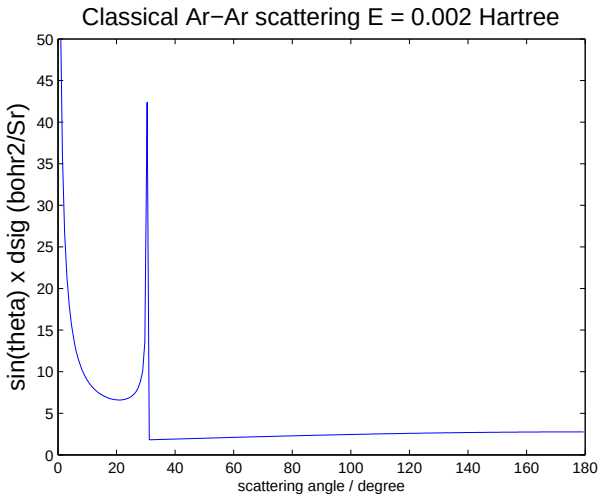

FIG. 6. Classical differential cross section, Ar–Ar scattering, $E = 0.002$.

Problem 9

Write a Matlab script to determine the classical differential cross section for the scattering of two Ar atoms at $E = 0.006$. You have previously written a script to determine $\theta(b)$, which you can use to obtain θ at a grid of values of b. Now, determine the derivative $d\theta/db$ using the Matlab function `gradient`, in other words

```
dth=gradient(th,db);
```

where `db` is the spacing of your impact parameter grid. Then determine the rainbow angle

```
[thr nr]=min(dth);thr=abs(thr);
```

Here, `nr` is the point in your array where the rainbow angle occurs. Next define a regular grid in angle, for example

```
dang=thr/30;angl=[1:dang:thr];angg=[thr:dang:pi];
```

Here, `angl` and `angg` (angle-lesser and angle-greater) are angular grids for angles less than and greater than the rainbow angle. Now, determine the range of the three branches of the deflection function, by executing

```
n=find(th>0);n=max(n);
```

Thus, `th(1:n)` corresponds to the positive branch of the deflection function, `th(n+1:nr)` corresponds to the negative branch inside the rainbow angle and `th(nr+1:nmax)` corresponds to the negative branch outside the rainbow angle. Interpolate the differential cross section from each of these branches onto the regular grid in angle

```
dcs1=abs(interp1(th(1:n),1./(sin(th(1:n)).*dth(1:n),angl,'cubic'));
dcs2=abs(interp1(th(1:n),1./(sin(th(1:n)).*dth(1:n),angg,'cubic'));
dcs3=abs(interp1(th(n+1:nr),1./(sin(th(n+1:nr)).*dth(n+1:nr),angl,'cubic'));
dcs4=abs(interp1(th(nr+1:nmax),1./(sin(th(nr+1:nmax)).*dth(nr+1:nmax),angl,'cubic'));
```

Then, add up `dcs1, dcs3,` and `dcs4` to obtain the differential cross section for $\theta \leq \theta_R$. The differential cross section for $\theta > \theta_R$ is given just by `dcs2`.

When you plot your result, make sure you multiply by $\sin\theta$. This will reduce the size of the singularities at $\theta = 0$ and $\theta = \pi$. The value of the dcs in the forward direction ($\theta = 0$) will still be very large, and dominate everything else on the plot. You can compensate for this by reducing the range of the y-axis on the plot using the command `plot(x,y,'ylim',[0 xx])` where `xx` is the maximum value of y that you wish to display.

IV. ELASTIC SCATTERING IN THREE DIMENSIONS: QUANTUM TREATMENT

A. Separation of radial and angular motion

In three dimensions the relative motion of two spherical particles subject to a potential which depends only on the magnitude of the distance between them can be reduced to the motion of the center of mass and the motion of an effective particle of mass $\mu = m_a m_b/(m_a + m_b)$ (where μ is called the "reduced mass") in the field of the potential $V(r)$. The corresponding Schrodinger equation is (outside of the potential, this is exactly the same as the equation for the motion of the electron in the H atom and the rotational motion of a diatomic molecule)

$$\left[-\frac{\hbar^2}{2\mu}\nabla^2 + V(r)\right]\psi(\mathbf{r}) = E\psi(\mathbf{r}) \tag{33}$$

Because $V(r)$ depends only on the magnitude of the distance between the two particles, we can expand the wavefunction as

$$\psi(\mathbf{r}) = \sum_{lm} Y_{lm}(\theta,\phi) g_l(r) = \sum_{lm} Y_{lm}(\theta,\phi) R_l(r)/r \tag{34}$$

where the radial function $R_l(r)$ satisfies the equation (we will drop the subscript l except when necessary)

$$\left(-\frac{\hbar^2}{2\mu}\frac{d^2}{dr^2} + \frac{\hbar^2 l(l+1)}{2\mu r^2} + V(r)\right) R(r) = E R(r) \tag{35}$$

Here, also, Y_{l0} is a spherical harmonic, which is related to the regular Legendre polynomial $P_l(\cos\theta)$ by

$$Y_{l0}(\theta,\phi) = \left(\frac{2l+1}{4\pi}\right)^{1/2} P_l(\cos\theta) \tag{36}$$

At large r, both the potential $V(r)$ and the centrifugal barrier go to zero, so that the radial function is the solution to the equation

$$d^2R(r)/dr^2 = -k^2 R(r)$$

and, thus, can be expressed either as linear combination of $\sin(kr)$ and $\cos(kr)$, or a linear combination of $\exp(ikr)$ and $\exp(-ikr)$. In most cases the potential goes to zero much faster

than r^2, so that (as in the case of the classical treatment of elastic scattering), it is useful to consider the behavior of this equation when $V(r)$ is zero, but not the centrifugal barrier. You can show that in this case we have

$$\lim_{r\to\infty} \text{Eq. (35)} = \left[x^2\frac{d^2}{dx^2} - l(l+1) + x^2\right] R(x) = 0 \tag{37}$$

where $x = kr$.

The solutions to this equation are related to the well-known spherical Bessel functions of the first and second kind: $j_l(x)$ and $y_l(x)$,[7] which themselves are solutions to the Hemlholz equation in spherical coordinates, namely

$$x^2\frac{d^2f}{dx^2} + 2x\frac{df}{dx} + \left[x^2 - l(l+1)\right] f_l(x) = 0$$

where $f_l(x)$ is either $j_l(x)$ or $y_l(x)$.

Problem 10

Show that the Ricatti-Bessel functions

$$\hat{j}_l(x) = xj_l(x)$$

and

$$\hat{y}_l(x) = xy_l(x)$$

Satisfy Eq. (37).

The spherical Bessel functions are related to the cylindrical Bessel functions $J_n(x)$ and $Y_n(x)$ through the relation

$$j_l(x) = \left[\frac{\pi}{2x}\right]^{1/2} J_{l+\frac{1}{2}}(x) \tag{38}$$

and, for the linearly independent Bessel function of the second kind

$$y_l(x) = \left[\frac{\pi}{2x}\right]^{1/2} Y_{l+\frac{1}{2}}(x) \tag{39}$$

B. Numerical determination of the scattering wavefunction

As r goes to zero, the potential becomes greater than the energy, so that the solution to the radial Schrodinger equation is either exponentially increasing or exponentially decreasing as $r \to 0$. We have to take the latter, since the wavefunction has to remain finite.

To obtain $R(r)$ everywhere, we start at small r, with an approximation to the correct exponentially decreasing function. If we assume that $V(r)$ is constant and large at $r = r_0$, then we can approximate

$$R(r_0) = 1 \times 10^{-10}$$

$$\left.\frac{dR}{dr}\right|_{r=r_0} = 1 \times 10^{-10}\kappa_0 \tag{40}$$

where $\kappa_0 = \left\{2\mu \left[V\left(r_0\right) - E\right]/\hbar^2\right\}^{1/2}$ If the spacing of our grid is h, then Eq. (40) allows us to write

$$R(r_1) = R(r_0) + \left.\frac{dR}{dr}\right|_{r=r_0} (r - r_0) = (1 + \kappa_0 h) \times 1 \times 10^{-10}$$

Here we implicitly assume that $R(r)$ behaves linearly in the first sector. Once we know the values of R_0 and R_1 we can use the Numerov method [Eq. (16)] to obtain $R(r)$ at all larger values of R.

Problem 11

Write a Matlab script to determine $R(r)$ for the collision of two Ar atoms at $E = 0.0005$. You can use the Numerov method to propagate the solution out to large r (probably $r = 20$ will be largely sufficient). The mass of Ar is 39.948 amu (the collision reduced mass is $\mu = m/2$).

At large r, the solution can be written as a linear combination of the two Ricatti-Bessel functions $\hat{y}_l(kr)$ and $\hat{j}_l(kr)$, namely

$$\lim_{r\to\infty} R(r) = \frac{1}{k}\left[A_l \hat{j}_l(kr) + B_l \hat{y}_l(kr)\right] \tag{41}$$

Here A_l and B_l are two arbitrary constants. Since both A and B are arbitrary, we have multiplied them both here by $1/k$, for convenience later.

If r_{N-1} and r_N are your two last grid points, then you can obtain the coefficients A_l and B_l by solving the set of linear equations (use Matlab's backslash function)

$$\begin{bmatrix} \hat{j}_l(kr_N) & \hat{y}_l(kr_N) \\ \hat{j}_l(kr_{N-1}) & \hat{y}_l(kr_{N-1}) \end{bmatrix} \begin{bmatrix} A_l \\ B_l \end{bmatrix} = \begin{bmatrix} kR(r_N) \\ kR(r_{N-1} \end{bmatrix} \tag{42}$$

You can obtain the values of the Ricatti-Bessel functions at r_N and r_{N-1} using Matlab's `besselj` and `bessely` commands for the cylindrical Bessel functions. [Remember to convert these to spherical Bessel functions using Eqs. (38) and (39)].

To check that everything is working, you should find that the values of the expansion coefficients A_l and B_l are converged with respect to decreasing r_0, increasing r_N, and increasing the size of the grid. Since the overall normalization of the wavefunction is arbitrary, we can avoid working with large numbers by renormalizing so that

$$A = \frac{A}{\sqrt{A^2 + B^2}} \text{ and } B = \frac{B}{\sqrt{A^2 + B^2}}$$

To test your Matlab code, Tab. III the values of A and B for Ar–Ar scattering at E=0.0005:

TABLE III. Asymptotic expansion coefficients, Ar–Ar scattering, E=0.0005 hartree.[a]

l	$\psi(R_N)$	A[b]	B[b]	S[c]
0	1.2708×10^{-7}	0.94857	–0.31662	0.79950–0.60067i
30	-5.3398×10^{-7}	–0.93076	0.36563	0.73263–0.68062i
80	-2.0026×10^{11}	0.99442	–0.10545	0.97776–0.20972i

[a] $\mu = 19.974$, $r_0 = 5.5$, $r_N = 25$, $h = 0.02$.
[b] renormalized.
[c] see Eq. (49)

When the centrifugal barrier becomes very large, so that

$$\frac{\hbar l(l+1)}{2\mu r^2} >> V(r)$$

then the Schrodinger equation for $R(r)$ [Eq. (35)] becomes identical to the equation for the Ricatti-Bessel functions [Eq. (37)]. The solution which behaves correctly at the origin ($\lim_{r\to 0} R(r) = 0$) is $\hat{j}_l(kr)$. Thus, at large l, the expansion coefficients are $\lim_{l\to\infty} A_l = 1$ and $\lim_{l\to\infty} B_l = 0$.

Now, from our numerical solution of the radial Schrodinger equation [Eq. (41)] we see that the large R behavior of the wavefunction is

$$\begin{aligned}\lim_{r\to\infty} \psi(\mathbf{r}) = \sum_{lm} Y_{lm}(\theta,\phi)\frac{R(r)}{r} &= \sum_l \frac{1}{kr}\left[A_l \hat{j}_l(kr_N) + B_l \hat{y}_l(kr_N)\right] Y_{l0}(\theta,\phi) \\ &= \sum_l \left[A_l j_l(kr_N) + B_l y_l(kr_N)\right] Y_{l0}(\theta,\phi) \\ &= \sum_l \left[\frac{2l+1}{4\pi}\right]^{1/2} \left[A_l j_l(kr_N) + B_l y_l(kr_N)\right] P_l(\cos\theta) \quad (43)\end{aligned}$$

Here, we have limited the sum just to the $m = 0$ projection states, because the scattering has cylindrical symmetry. By equating Eqs. (68) and (43), we can obtain the coefficients in the expansion of the scattering amplitude in terms of the coefficients A_l and B_l, which we have obtained numerically.

To do so, we need first examine the asymptotic properties of the Ricatti-Bessel functions. Since

$$\lim_{x\to\infty} J_\nu(x) = \left[\frac{2}{\pi x}\right]^{1/2} \cos\left(x - \frac{1}{2}\nu\pi - \frac{1}{4}\pi\right)$$

so that

$$\lim_{x\to\infty} J_{l+\frac{1}{2}}(x) = \left[\frac{2}{\pi x}\right]^{1/2} \cos\left[x - (l+1)\frac{\pi}{2}\right]$$

we find

$$\lim_{x\to\infty} j_l(x) = \frac{1}{x}\cos\left[x - (l+1)\frac{\pi}{2}\right] \quad (44)$$

and, similarly (you should show this)

$$\lim_{x\to\infty} y_l(x) = \frac{1}{x}\sin\left[x - (l+1)\frac{\pi}{2}\right] \quad (45)$$

Rather than use the real spherical Bessel functions, we can use the complex spherical

Hankel functions, namely

$$h_l^{(1,2)}(x) = j_l(x) \pm i y_l(x) \tag{46}$$

where the first (second) spherical Hankel functions corresponds to the plus (minus) sign.

Problem 12

Use Eq. (46) to show that the asymptotic ($r \to \infty$) behavior of these two spherical Hankel functions is given by

$$\lim_{r\to\infty} h_l^{(1,2)}(kr) = \frac{1}{kr} \exp\left\{\pm i\left[kr - (l+1)\pi/2\right]\right\} = \frac{(\mp i)^{l+1}}{kr} e^{\pm ikr} \tag{47}$$

Problem 13

The behavior of the Bessel functions at very large r is given by Eqs. (44) and (45). Show that

$$\begin{aligned}\lim_{r\to\infty} \frac{R(r)}{r} &= \frac{1}{2kr}\left[(A_l - iB_l)\hat{h}_l^{(1)} + (A_l + iB_l)\hat{h}_l^{(2)}\right] \\ &= \frac{1}{2}\left[(A_l - iB_l)h_l^{(1)} + (A_l + iB_l)h_l^{(2)}\right]\end{aligned} \tag{48}$$

You can re-arrange this equation to write

$$\lim_{r\to\infty} \frac{R(r)}{r} = C_l\left[S_l h_l^{(1)}(kr) + h_l^{(2)}(kr)\right] \tag{49}$$

where C_l and S_l are complex constants.

Problem 14

Determine an expression which relates the constant S_l to the constants A_l and B_l which you obtain from your Numerov propagation.

See if you can derive any limits on the magnitude of the S coefficient Now, from the answer to Problem 13 we see that

$$\lim_{r\to\infty}\frac{R(r)}{r}=\frac{1}{kr}C\left[(-i)^{l+1}e^{ikr}S_l+i^{l+1}e^{-ikr}\right] \tag{50}$$

Insertion of this equation into Eq. (43) leads to

$$\begin{aligned}\lim_{r\to\infty}\psi(\mathbf{r})&=\sum_{lm}Y_{lm}(\theta,\phi)\lim_{r\to\infty}\frac{R(r)}{r}=\sum_l\left[\frac{2l+1}{4\pi}\right]^{1/2}P_l(\cos\theta)\lim_{r\to\infty}\frac{R(r)}{r}\\&=\sum_l\left[\frac{2l+1}{4\pi}\right]^{1/2}\frac{1}{kr}C\left[(-i)^{l+1}e^{ikr}S_l+i^{l+1}e^{-ikr}\right]P_l(\cos\theta)\\&=\sum_l\left[\frac{2l+1}{4\pi}\right]^{1/2}\frac{i}{kr}C\left[-(-i)^{l}e^{ikr}S_l+i^{l}e^{-ikr}\right]P_l(\cos\theta)\end{aligned} \tag{51}$$

C. Phase shift

From Eqs. (41), (44), and (45), we see that at large R we can write

$$\begin{aligned}\lim_{r\to\infty}R(r)&\sim A_l\cos\left[kr-\frac{\pi}{2}(l+1)\right]+B_l\sin\left[kr-\frac{\pi}{2}(l+1)\right]\\&\sim A_l\sin\left(kr-l\pi/2\right)+B_l\cos\left(kr-l\pi/2\right)\end{aligned} \tag{52}$$

Equivalently, we can write

$$\lim_{r\to\infty}R(r)\sim D\sin\left(kr-l\pi/2+\delta_l\right) \tag{53}$$

where δ_l is the "phase shift".

Problem 15

Show that

$$\delta_l = \tan^{-1}\left(\frac{B}{A}\right) \tag{54}$$

Then, show that

$$S_l = \exp(2i\delta_l) \tag{55}$$

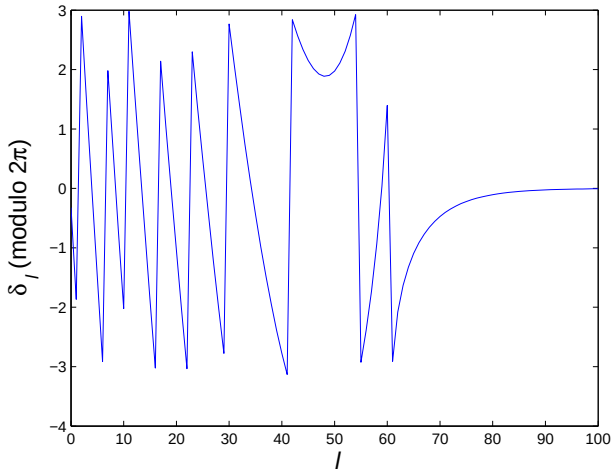

FIG. 7. Phase shift (modulo 2π) for Ar–Ar scattering, $E = 0.0005$ hartree.

In pratice, determination of the phase shift from Eq. (54) gives the value of δ_l only to within modulo 2π, as seen in Fig. (7).

One can unroll this by hand, starting at large l, where the phase shift is zero, and progressively adding or subtracting 2π so that the resulting phase shift is smooth, as shown in Fig. (8).

For $V(r) = 0$, the solution to the Schrodinger equation is $R(r) = \hat{A} j_l(kr)$, because the other linearly independent solution $\hat{y}_l(kr)$ blows up at the origin. Thus, for $V(r) = 0$, $A = 1$ and $B = 0$, so that $\delta_l = 0$. At large l, the attractive well in the potential pulls the wavefunction in (as compared to the $V(r) = 0$ case, so that there are more oscillations

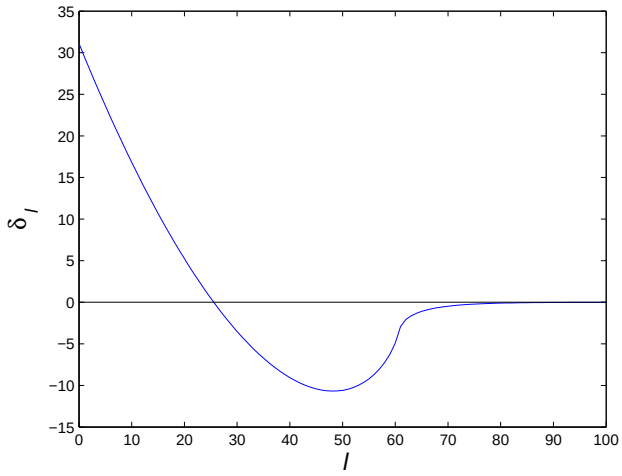

FIG. 8. Phase shift for Ar–Ar scattering, $E = 0.0005$ hartree.

than would be seen in the absence of a potential. This is illustrated by Fig. (9). The corresponding phase shift is negative.

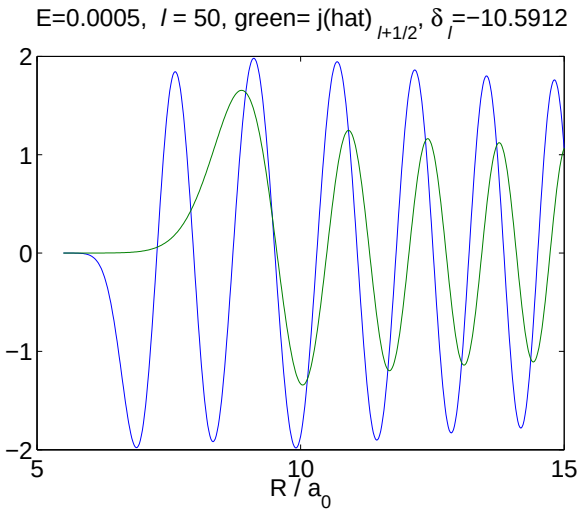

FIG. 9. Scattering wavefunction $R(r)$ (blue) for Ar–Ar scattering, $E = 0.0005$ hartree, $l = 50$. The green curve is the corresponding Ricatti-Hankel function, which is the wavefunction for $V(r) = 0$. The phase shift is $\sim -1.5 \times 2\pi$ which indicates, as seen here, that there are approximately 1.5 additional full oscillations in the blue curve.

As l decreases, the centrifugal barrier is less important, relative to $V(r)$, so that the repulsive part of the potential pushes the wavefunction out, so that there are fewer oscillations as compared to the $V(r) = 0$ case. This is seen in Fig. (10). The corresponding phase shift

is positive.

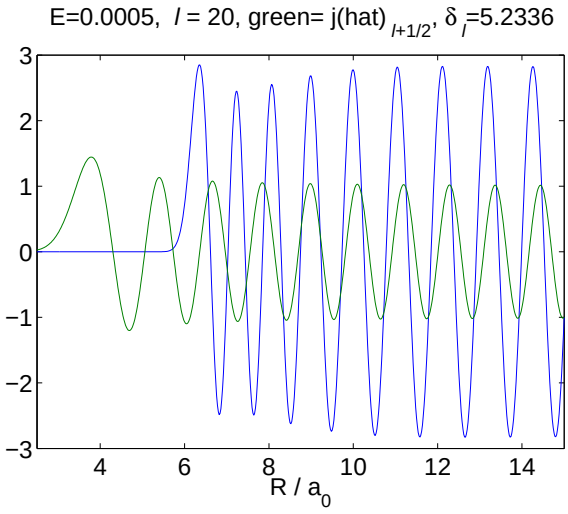

FIG. 10. Scattering wavefunction $R(r)$ (blue) for Ar–Ar scattering, $E = 0.0005$ hartree, $l = 20$. The green curve is the corresponding Ricatti-Hankel function, which is the wavefunction for $V(r) = 0$. The phase shift is $\sim 0.8 \times 2\pi$ which indicates that there is approximately one fewer full oscillation in the MidnightBlue curve.

In a semiclassical description, the phase shift is 2π times the difference between the number of wavelengths in the path followed if the potential $V(r)$ is zero compared to the number of wavelengths in the actual path, namely

$$\delta_l = 2\pi \lim_{r\to\infty} \left[\int_{V=0\,\mathrm{path}} \frac{dr}{\lambda_r} - \int_{\mathrm{actual\,path}} \frac{dr}{\lambda_r} \right] \tag{56}$$

where λ_r is the local deBroglie wavelength

$$\lambda_r = \frac{h}{p(r)} = \frac{h}{\mu v(r)}$$

with, from Eq. (25)

$$\mu v(r) = \mu \dot{r} = \left\{ 2E\mu \left[1 - \frac{b^2}{r^2} - \frac{V(r)}{E} \right] \right\}^{1/2} = \mu v \left[1 - \frac{b^2}{r^2} - \frac{V(r)}{E} \right]^{1/2} \tag{57}$$

with μv being the initial relative momentum $\left[\mu v = (2\mu E)^{1/2} \right]$. The lower range of integration is the classical turning point r_{min} (in the case where the potential is zero, the turning point

is equal to the impact parameter) so that

$$\delta_l = \frac{\mu v}{\hbar}\left[\int_b^R \left[1-\frac{b^2}{r^2}\right]^{1/2} dr - \int_{r_{min}}^R \left[1-\frac{b^2}{r^2}-\frac{V(r)}{E}\right]^{1/2} dr\right] \tag{58}$$

Here, R is the value of the distance for which the potential has effectively vanished (see Sec. II.B). The first integral can be evaluated analytically to give [8]

$$\int_b^R \left[1-\frac{b^2}{r^2}\right]^{1/2} dr = \left(R^2-b^2\right)^{1/2} - b\cos^{-1}(b/R)$$

In order to evaluate numerically both integrals, we need to know the correspondence between the classical impact parameter and the quantum mechanical angular momentum. We remember from Eq. (23) that $l_{cl}^2 = (\mu v b)^2$. We also know that square of the angular momentum in quantum mechanics is $\left\langle \hat{l}^2 \right\rangle = l(l+1)\hbar^2$. Thus, in Eq. (58) we need to replace b^2 by

$$b^2 = \frac{\hbar^2 l(l+1)}{(\mu v)^2}$$

Thus, Eq. (58) becomes (in atomic units, where $\hbar = 1$)

$$\begin{aligned}
\delta_l &= \mu v\left[\int_b^R \left[1-\frac{l(l+1)}{\mu v r^2}\right]^{1/2} dr - \int_{r_{min}}^R \left[1-\frac{l(l+1)}{(\mu v r)^2}-\frac{V(r)}{E}\right]^{1/2} dr\right] \\
&= \mu v\left[\left(R^2-b^2\right)^{1/2} - b\cos^{-1}\left(\frac{b}{R}\right) - \int_{r_{min}}^R \left[1-\frac{l(l+1)}{(\mu v r)^2}-\frac{V(r)}{E}\right]^{1/2} dr\right] \\
&= \mu v\left[\left(R^2-b^2\right)^{1/2} - b\cos^{-1}\left(\frac{b}{R}\right) - \int_{r_{min}}^R \left[1-\frac{b^2}{r^2}-\frac{V(r)}{E}\right]^{1/2} dr\right]
\end{aligned} \tag{59}$$

where, here $b = [l(l+1)]^{1/2}/\mu v$.

Problem 16

Write a Matlab script to determine the semiclassical phase shift, defined in the preceding equation. Use the work you did in Problem 6 to determine the turning point, then use the Matlab function `quad` to evaluate the integral.

For Ar–Ar collisions at $E = 0.0005$ hartree, the semiclassical phase shift, as a function of

l, differs only minutely from the quantum phase shift shown in Fig. (8). The following table contains some numerical comparisons.

TABLE IV. Comparison of quantum and semi-classical phase shifts (radians) for Ar–Ar scattering, E=0.0005 hartree.

l	δ_Q [Eq. (54)]	δ_{SC} [Eq. (59)]
0	31.09	31.87
20	5.23	5.23
40	–9.06	–9.07
60	–4.89	–5.01

Typically, semi-classical approximations become less accurate when the mass is reduced. If we replace the mass of Ar with that of He, and simulate He–He collisions at $E = 0.0005$ hartree with the Ar–Ar potential, the reduced mass drops form ~ 20 to ~ 2, a factor of 10. However, as shown by Fig. 11 the agreement is still excellent, with a few slight exceptions, notably at $l = 0$.

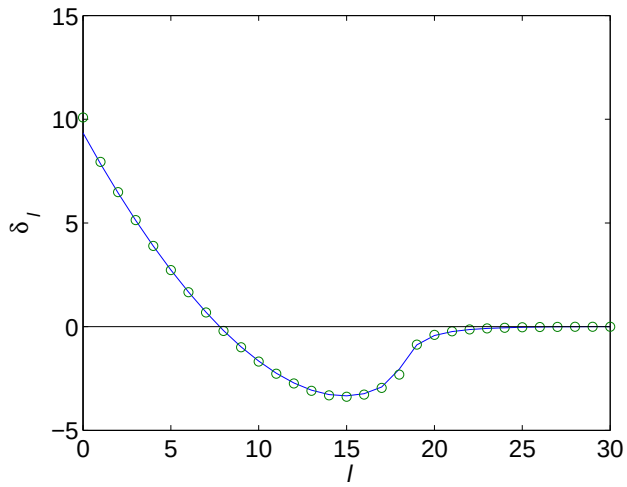

FIG. 11. Phase shift for He–He scattering with the Ar–Ar potential, $E = 0.0005$ hartree. The MidnightBlue curve is the quantum predictions from Eq. (54) and the green circles are the semiclassical predictions from Eq. (59). Note that the minimum occurs at $l \cong 15$, while the minimum in Fig. (8) occurs at $l \cong 50$. This is because for a lighter reduced mass the value of l which corresponds to a given impact parameter is smaller.

D. Scattering boundary conditions

The Schrodinger equation is solved subject to the boundary condition

$$\lim_{r\to\infty} \psi(\mathbf{r}) = e^{ikz} + \frac{f(\theta)e^{ikr}}{kr} \tag{60}$$

The first term corresponds to an incoming plane wave and the second term, to the scattered wave. [9]

The flux density can be evaluated as

$$\vec{J} = -\frac{i\hbar}{2\mu}\left(\psi^*\nabla\psi - \psi\nabla\psi^*\right) \tag{61}$$

The incoming flux is evaluated by using $\psi_i = e^{ikz}$ which yields

$$J_i\hat{z} = \frac{\hbar k}{\mu}\hat{z}$$

This is the incoming flux per unit area ($dA = dxdy$). The outgoing flux through a sphere of radius r can be evaluated by using $\psi_o = f(\theta)e^{ikr}/r$ and knowing that the radial component of the gradient in spherical polar coordinates is

$$\hat{r}\frac{d}{dr}$$

This yields

$$J_o\hat{r} = \left(\frac{\hbar}{k\mu}|f(\theta)|^2/r^2\right)\hat{r} \tag{62}$$

The total outgoing flux through the surface of a sphere of radius r is

$$\int J_o r^2 d\Omega$$

Since the scattering is independent of the azimuthal angle (by symmetry) we see that the outgoing flux per unit solid angle is

$$J_o(\Omega) = \frac{\hbar}{k\mu}|f(\theta)|^2$$

Since the differential cross section is defined (see Sec. III) as the ratio of the outgoing flux per unit solid angle to the incoming flux per unit area, we see that

$$\frac{d\sigma}{d\Omega} \equiv J_o/J_i = \frac{|f(\theta)|^2}{k^2} \tag{63}$$

The quantity $f(\theta)$ is called the "scattering amplitude."

E. Determination of $f(\theta)$

To obtain the scattering amplitude, we first use the well-known expansion of a plane wave in spherical waves (due originally to Lord Rayleigh) namely

$$e^{ikz} = \sum_l i^l \left[4\pi(2l+1)\right]^{1/2} j_l(kr) Y_{l0}(\theta, \phi) \tag{64}$$

where we see the spherical Bessel function one more time. From Eq. (36), we see that Eq. (64) can be rewritten in terms of Legendre polynomials as

$$e^{ikz} = \sum_l i^l (2l+1) j_l(kr) P_l(\cos\theta) \tag{65}$$

Similarly, we can expand the scattering amplitude in a Legendre series

$$f(\theta) = \sum_l \frac{1}{2}(2l+1) f_l P_l(\cos\theta) = i \sum_l \frac{1}{2i}(2l+1) f_l P_l(\cos\theta) \tag{66}$$

Because of the orthogonality properties of the Legendre polynomials

$$\int_0^\pi P_l(\cos\theta) P_m(\cos\theta) \sin\theta d\theta = \frac{2\delta_{lm}}{2l+1} \tag{67}$$

we see that

$$f_l = \int_0^\pi P_l(\cos\theta) f(\theta) \sin\theta d\theta$$

Consequently, the asymptotic behavior of the wavefunction [Eq. (60)] can be re-expressed as

$$\lim_{r\to\infty}\psi(\mathbf{r}) = \sum_l (2l+1)\left[\frac{1}{2}f_l\frac{e^{ikr}}{kr} + i^l j_l(kr)\right]P_l(\cos\theta) \tag{68}$$

From Eq. (46) we see that

$$j_l(kr) = \frac{1}{2}\left[h_l^{(1)}(kr) + h_l^{(2)}(kr)\right]$$

With this, along with Eq. (47), we can rewrite Eq. (68) as

$$\lim_{r\to\infty}\psi(\mathbf{r}) = \frac{1}{2}\frac{i}{kr}\sum_l (2l+1)\left[e^{ikr}\left(\frac{f_l}{i} - 1\right) + (-1)^l e^{-ikr}\right]P_l(\cos\theta) \tag{69}$$

Problem 17

Check all the algebra and derivations. Now, the asymptotic expression for the wavefunction you have obtained by numerical solution [Eq. (51)] must equal this expression. Knowing this, for each l equate the coefficients of $\exp(ikr)$ and $\exp(-ikr)$ in Eqs. (51) and (69) to derive an equation for the terms f_l in the expansion of the scattering amplitude in terms of the coefficient S_l. By requiring that the coefficients of $\exp(-ikr)$ be identical in Eqs. (51) and (69), you can show that

$$C_l = i^l\left[(2l+1)\pi\right]^{1/2} \tag{70}$$

and

$$f_l = i(1 - S_l) \tag{71}$$

Requiring the coefficient of $\exp(-ikr)$ to be identical, yields Eq. (71).

Problem 18

Modify your Matlab script to obtain as a function of l the scattering amplitude from this equation at all values of l. As l increases, S_l goes to $+1$, so that $\lim_{l\to\infty} f_l = 0$. Then,

using Eq. (63) determine the differential cross section for Ar–Ar scattering at E=0.0005. Do a similar calculation for He–He scattering ($\mu = 2.0013$ amu) described by the Ar–Ar potential. In both cases, compare your results with the classical differential cross section plotted in Fig. 6.

Table V lists some Ar–Ar scattering amplitudes

TABLE V. Comparison of quantum scattering amplitudes and differential cross section for Ar–Ar scattering, E=0.0005 hartree, l_{max}=100.

θ	$f(\theta)$	$d\sigma/d\Omega$ [a]
2	1.0522e+3 + 9.5366e+1 i	30655
22	5.5310e+1 + 6.1524e+1 i	187.98
42	–4.0047e+1 + 3.1983e+1 i	72.14
62	–1.4737e+1 + 2.8595e+1 i	28.42

[a] Eq. (63); Units of a_0^2/Sr.

Here is a plot of the differential cross sections for Ar–Ar and for He–He (with the Ar–Ar potential).

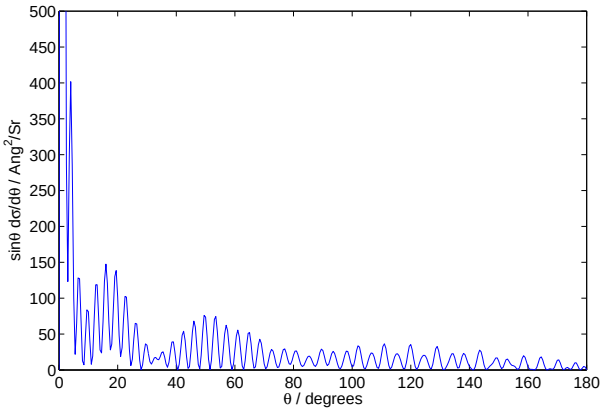

FIG. 12. Differential scattering of two Ar atoms, $E = 0.0005$ hartree.

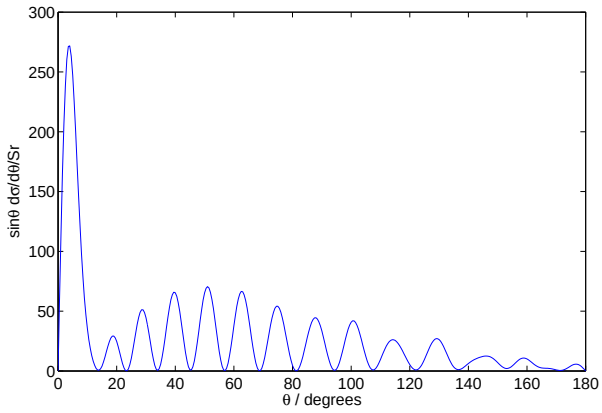

FIG. 13. Differential scattering of two He atoms, $E = 0.0005$ hartree.

F. Integral Cross Section

The integral over all solid angle of the differential cross section defines the "integral" cross section, namely

$$\sigma = \int \frac{d\sigma}{d\Omega} \sin\theta d\theta d\phi = 2\pi \int \frac{d\sigma}{d\Omega} \sin\theta d\theta = \frac{2\pi}{k^2} \int |f(\theta)|^2 \sin\theta d\theta =$$

Here, because the scattering is azimuthally symmetric, we have integrated trivially over ϕ.

Problem 19

Show that if you substitute the expansion over l of $f(\theta)$ [Eq. (66)] and use the orthogonality of the Legendre polynomials [Eq. (67)], you obtain

$$\sigma = \frac{\pi}{k^2} \sum_l (2l+1)|f_l|^2 = \frac{\pi}{k^2} \sum_l (2l+1)|1 - S_l|^2 \tag{72}$$

Using Eqs. (55), show that this is equivalent to

$$\sigma = \frac{2\pi}{k^2} \sum_l (2l+1) \sin^2 \delta_l \tag{73}$$

Then, use this equation, as well as Eqs. (55), (66), and the relationship $P_l(\theta = 0) = 1$ to prove the "optical theorem" which states that the integral cross section is proportional

to the imaginary part of the amplitude for scattering in the forward ($\theta = 0$) direction. [10]

$$\sigma = \frac{4\pi}{k^2}\mathrm{Im}[f(\theta = 0)] \tag{74}$$

V. INELASTIC SCATTERING

A. Generalities

Suppose you scatter an atom with internal states ψ_i, which satisfy the Schrodinger equation

$$H_{int}(q)\chi_n(q) = \varepsilon_n\chi_n(q) \tag{75}$$

where q designates the internal degrees of freedom and ε_n is the internal energy of state n. The eigenfunctions $\chi_n(q)$ are, of course, orthonormal, namely

$$\int \chi_n^*(q)\chi_m(q)dq = \delta_{mn}$$

The corresponding time-independent Schrodinger equation for the system of the atom plus a structureless collision partnerthen becomes

$$\left[-\frac{\hbar^2}{2\mu}\nabla^2 + H(r,q)\right]\psi(\mathbf{r},q) = E\psi(\mathbf{r},\mathbf{q}) \tag{76}$$

where $H(r,q)$ is some Hamiltonian which depends on both the separation of the atom with its collision partner and the internal degrees of freedom of the atom. We shall assume for simplicity here that H depends only the the magnitude of r, not its orientation. In the limit of large separation,

$$\lim_{r\to\infty} H(r,q) = H_{int}(q) \tag{77}$$

Similarly, the wavefunction depends on both the internal degree(s) of freedom and the

separation coordinate r. Extending Eq. (**??**), we will expand the wavefunction as

$$\psi(\mathbf{r},q) = \sum_n \sum_{lm} Y_{lm}(\theta,\phi) g_{ln}(r) \chi_n(q) = \sum_n \sum_{lm} Y_{lm}(\theta,\phi) \frac{C_{ln}(r)}{r} \chi_n(q) \tag{78}$$

Now, substitute this expansion into Eq. (76), then premultiply by one of the internal state functions, $\chi_m(q)$, say, and integrate over q. You can show that the Schrodinger equation is then transformed into a set of coupled ordinary differential equations

$$\left[-\frac{\hbar^2}{2\mu} \frac{d^2}{dr^2} + \frac{\hbar^2 l(l+1)}{2\mu r^2} + V_{mm}(r) - E \right] C_m(r) = -\sum_{n \neq m} V_{mn}(r) C_n(r) \,, \tag{79}$$

where

$$V_{mn}(r) = \int \chi_m^*(q) H(r,q) \chi_n(q) dq \tag{80}$$

Note that for convenience in the notation later in the section we are using $C(r)$ rather than $R(r)$ to designate the radial wavefunctions divided by r.

Formally, we can rewrite these so-called "close-coupled" equations as

$$\left[\mathbf{I} \frac{d^2}{dr^2} + \mathbf{W}(r) \right] \mathbf{C}(r) = 0 \tag{81}$$

where

$$\mathbf{W}(r) = 2\mu \left[E\mathbf{I} - \mathbf{V}(r) \right] \tag{82}$$

In this equation, and henceforth, we use atomic units, where $\hbar = 1$.

The solution to Eq. (81) is a matrix, with each column representing a linearly independent solution involving coefficients C_{nm} for all n internal states. For the case where there are only two internal states,

$$\mathbf{C}(r) = \begin{bmatrix} C_{11}(r) & C_{12}(r) \\ C_{21(r)} & C_{22}(r) \end{bmatrix} \tag{83}$$

Equation (77) implies that asymptotically the $\mathbf{W}(r)$ matrix is diagonal with elements

$$\lim_{r\to\infty} W_{nn}(r) = k_n^2 \equiv 2\mu \left[E - \varepsilon_n - \frac{l(l+1)}{R^2} \right] \tag{84}$$

The appropriate scattering boundary conditions in this two-channel case is

$$\lim_{r\to\infty}\mathbf{C}(r) = \begin{bmatrix} k_1^{-1/2}\hat{h}_{l_1}^{(2)}(k_1r) & 0 \\ 0 & k_2^{-1/2}\hat{h}_{l_2}^{(2)}(k_2r) \end{bmatrix} - \begin{bmatrix} k_1^{-1/2}\hat{h}_{l_1}^{(1)}(k_1r) & 0 \\ 0 & k_2^{-1/2}\hat{h}_{l_2}^{(1)}(k_2r) \end{bmatrix} \mathbf{S} \tag{85}$$

Here the S coefficient is now an S matrix. In matrix notation, Eq. (85) is

$$\lim_{r\to\infty}\mathbf{C}(r) = \hat{\mathbf{h}}^{(2)}(r) - \hat{\mathbf{h}}^{(1)}(r)\mathbf{S} \tag{86}$$

In the case where the angular momentum l is zero, Eq. (85) goes to

$$\lim_{r\to\infty}\mathbf{C}(r) = i\begin{bmatrix} k_1^{-1/2}\exp(-ik_1r) & 0 \\ 0 & k_2^{-1/2}\exp(-ik_2r) \end{bmatrix} + i\begin{bmatrix} k_1^{-1/2}\exp(ik_1r) & 0 \\ 0 & k_2^{-1/2}\exp(ik_2r) \end{bmatrix} \mathbf{S} \tag{87}$$

B. The renormalized Numerov method in the asymptotic basis

Given the potential, how do we obtain the S matrix? We set up a regular grid of $N+1$ points, with h the width of each sector. At the first point, which is presumed to lie well within the classically forbidden region, we will assume that the wavefunction vanishes, in other words

$$\mathbf{C}(r_0) \equiv C_0 = \begin{bmatrix} 0 & 0 \\ 0 & 0 \end{bmatrix} \tag{88}$$

To propagate the solution we can use the Numerov algorithm [Eq. (16)], namely (for a one-dimensional problem)

$$(1 - T_{M+1})\, C_{M+1} = (2 + 10T_M)\, C_M - (1 - T_{M-1})\, C_{M-1} \tag{89}$$

where

$$T_M = -\frac{h^2}{12} W(r_M) = -\frac{h^2}{12} 2\mu \left[E - V(r = r_M)\right] \tag{90}$$

Because the kinetic energy is diagonal, this same three-term recursion relation can be easily generalized to multidimensional problems. Note the difference between Eq. (16) and (89). In the former case the T terms are defined as $E-V$, whereas here, to be consistent with Ref. [11], we define the T terms as $V - E$. For a multi-state (sometimes called "multichannel") problem, Eqs. (89) and (90) are written in matrix notation, namely

$$\left(\mathbf{I} - \mathbf{T}_{M+1}\right) \mathbf{C}_{M+1} = \left(2\mathbf{I} + 10\mathbf{T}_M\right) \mathbf{C}_M - \left(\mathbf{I} - \mathbf{T}_{M-1}\right) \mathbf{C}_{M-1} \tag{91}$$

and

$$\mathbf{T}_M = -\frac{h^2}{12} 2\mu \left[E\mathbf{I} - \mathbf{V}(r = r_M)\right] \tag{92}$$

In order to avoid the numerical instabilities caused by exponentially growing solutions in the classically forbidden region, we shall use the "renormalized" Numerov algorithm, due to Johnson. [12] To derive the propagation algorithm, we introduce two transformations. First, we define

$$\mathbf{F}_M = \left(\mathbf{I} - \mathbf{T}_M\right) \mathbf{C}_M \tag{93}$$

so that the basic propagation relation [Eq. (89)] becomes

$$\mathbf{F}_{M+1} - \mathbf{U}_M \mathbf{F}_M + \mathbf{F}_{M-1} = 0 \tag{94}$$

where

$$\mathbf{U}_M = \left(2\mathbf{I} + 10\mathbf{T}_M\right) \left(\mathbf{I} - \mathbf{T}_M\right)^{-1} \tag{95}$$

Note that we will use subscript "M" to designate the M^{th} sector or the M^{th} grid point R_M, while we use subscripts n and m as as row and column indices.

Now, we define the "ratio matrix"

$$\mathbf{R}_{M+1} = \mathbf{F}_{M+1} \mathbf{F}_M^{-1} = \left(\mathbf{I} - \mathbf{T}_{\mathbf{M+1}}\right) \mathbf{C}_{M+1} \left[\left(\mathbf{I} - \mathbf{T}_{\mathbf{M}}\right) \mathbf{C}_M\right]^{-1} \tag{96}$$

It follows that $\mathbf{F}_{M+1} = \mathbf{R}_{M+1} \mathbf{F}_M$ and $\mathbf{R}_M^{-1} = \mathbf{F}_{M-1} \mathbf{F}_M^{-1}$. Solving for $\mathbf{R}$ rather than $\mathbf{C}$ will eliminate instabilities in the original Numerov method due to exponentially growing

solutions in the classically forbidden region.

This allows you to rewrite the equation for the ratio matrix [Eq. (96)] as

$$\mathbf{R}_{M+1} = \mathbf{U}_M - \mathbf{R}_M^{-1} \tag{97}$$

This is a two-term recursion relation for the ratio matrix.

Propagation of the ratio matrix can be accomplished provided we specify the inverse of $\mathbf{R}$ at the first grid point, namely $\mathbf{R}_0^{-1}$. To do so we assume that the solution at the first grid point vanishes [Eq. (88)]. At the second grid point, the solution will be small but not zero. Consequently, $\mathbf{F}_0 = \mathbf{0}$ and $\mathbf{F}_1 \neq \mathbf{0}$. This implies that $\mathbf{R}_0^{-1} = \mathbf{0}$. Thus,

$$\mathbf{R}_1 = \mathbf{U}_0 \tag{98}$$

and

$$\mathbf{R}_2 = \mathbf{U}_1 - \mathbf{R}_1^{-1} = \mathbf{U}_1 - \mathbf{U}_0^{-1} \tag{99}$$

Subsequently, the two-term recursion relation [Eq. (97)] can be used to determine the ratio matrix all the way until the last grid point.

Since $\mathbf{W}$ is symmetric, it follows that both $\mathbf{T}$ and $\mathbf{U}$ are symmetric. Since $\mathbf{R}_0^{-1} = \mathbf{0}$, which is symmetric, the $\mathbf{R}$ matrix continues to be symmetric throughout the propagation.

We can also show that [see Eq. (95)],

$$\mathbf{U}_M = (2\mathbf{I} + 10\mathbf{T}_M)\,(\mathbf{I} - \mathbf{T}_M)^{-1} = 12(\mathbf{I} - \mathbf{T}_M)^{-1} - 10\mathbf{I} \tag{100}$$

This along with Eq. (97) define the propagation from grid point M to grid point $M+1$. Knowing the ratio matrix at grid point M ($\mathbf{R}_M$), as well as $\mathbf{U}_M$ from Eq. (100), we can compute $\mathbf{R}_{M+1}$. The overall propagation relation is then

$$\begin{aligned}\mathbf{R}_{M+1} &= -\mathbf{R}_M^{-1} + 12\,(\mathbf{I} - \mathbf{T}_M)^{-1} - 10\mathbf{I} \\ &= -\mathbf{R}_M^{-1} + 12\left(\mathbf{I} + \frac{h^2}{12}\mathbf{W}_M\right)^{-1} - 10\mathbf{I}\end{aligned} \tag{101}$$

This involves two matrix inversions per sector.

Problem 20

Show that if we assume $\mathbf{F}_0 = \mathbf{0}$ and $\mathbf{F}_1 \neq \mathbf{0}$, then $\mathbf{R}_0^{-1} = \mathbf{0}$.

C. Determination of the log-derivative matrix

Extraction of the S matrix is most easily done if one first determines the log-derivative matrix at the end of the last sector. This is defined as a multi-channel generalization of the logarithmic derivative of the wavefunction, namely

$$\mathbf{Y}_N = \mathbf{C}_N{}'\mathbf{C}_N^{-1}$$

For this we will need the derivative of the solution. We know, by application of a standard Taylor expansion,

$$\psi(r+h) = \psi(r) + h\left.\frac{d\psi}{dr}\right|_r + \frac{h^2}{2}\left.\frac{d^2\psi}{dr^2}\right|_r + \frac{h^3}{6}\left.\frac{d^3\psi}{dr^3}\right|_r$$

and, similarly

$$\psi(r-h) = \psi(r) - h\left.\frac{d\psi}{dr}\right|_r + \frac{h^2}{2}\left.\frac{d^2\psi}{dr^2}\right|_r - \frac{h^3}{6}\left.\frac{d^3\psi}{dr^3}\right|_r$$

By subtracting these two equations you can obtain

$$\left.\frac{d\psi}{dr}\right|_{r=r_N} \approx \frac{\psi_{N+1} - \psi_{N-1}}{2h} - \frac{h^2}{6}\left.\frac{d^3\psi}{dr^3}\right|_{r=r_N} + \mathcal{O}\left(h^5\left.\frac{d^5\psi}{dr^5}\right|_{r=r_N}\right) \tag{102}$$

Now

$$\left.\frac{d^3\psi}{dr^3}\right|_{r=r_N} \approx \frac{\psi''_{N+1} - \psi''_{N-1}}{2h} = \frac{-W_{N+1}\psi_{N+1} + W_{N-1}\psi_{N-1}}{2h}$$

Here we have used Eq. (81) to simplify the right hand side of the last equation.

We can neglect the terms of $\mathcal{O}(h^5)$ to obtain

$$\left.\frac{d\psi}{dr}\right|_{r=r_N} \approx \frac{1}{2h}(\psi_{N+1} - \psi_N) + \frac{h}{12}\left(W_{N+1}\psi_{N+1} - W_{N-1}\psi_{N-1}\right)$$

$$= \frac{1}{h}\left[\left(\frac{1}{2}+\frac{h^2}{12}W_{N+1}\right)\psi_{N+1} - \left(\frac{1}{2}+\frac{h^2}{12}W_{N-1}\right)\psi_{N-1}\right]$$

$$= \frac{1}{h}\left[\left(\frac{1}{2}-T_{N+1}\right)\psi_{N+1} - \left(\frac{1}{2}-T_{N-1}\right)\psi_{N-1}\right] \tag{103}$$

We can generalize this to our matrix representation of the solution in the case of coupled equations obtaining

$$\mathbf{C}_N{}' = \frac{1}{h}\left[\left(\frac{1}{2}\mathbf{I}-\mathbf{T}_{N+1}\right)\mathbf{C}_{N+1} - \left(\frac{1}{2}\mathbf{I}-\mathbf{T}_{N-1}\right)\mathbf{C}_{N-1}\right] \tag{104}$$

The derivation of the formula for the derivative in Eq. (103) was first given by Blatt [13] and follows closely the procedure used in deriving the original Numerov method. [14]

At the end of the last sector we obtain $\mathbf{R}_{N+1}$ from $\mathbf{R}_N^{-1}$. We know that

$$\mathbf{R}_{N+1} = \mathbf{F}_{N+1}\mathbf{F}_N^{-1} = \left(\mathbf{I}-\mathbf{T}_{N+1}\right)\mathbf{C}_{N+1}\left[\left(\mathbf{I}-\mathbf{T}_N\right)\mathbf{C}_N\right]^{-1}$$

and

$$\mathbf{R}_N = \mathbf{F}_N\mathbf{F}_{N-1}^{-1} = \left(\mathbf{I}-\mathbf{T}_N\right)\mathbf{C}_N\left[\left(\mathbf{I}-\mathbf{T}_{N-1}\right)\mathbf{C}_{N-1}\right]^{-1}$$

From the first of these two equations we obtain

$$\mathbf{C}_{N+1} = \left(\mathbf{I}-\mathbf{T}_{N+1}\right)^{-1}\mathbf{R}_{N+1}\left(\mathbf{I}-\mathbf{T}_N\right)\mathbf{C}_N$$

and from the second, we obtain

$$\mathbf{C}_{N-1} = \left(\mathbf{I}-\mathbf{T}_{N-1}\right)^{-1}\mathbf{R}_N^{-1}\left(\mathbf{I}-\mathbf{T}_N\right)\mathbf{C}_N$$

If we substitute these two equations into Eq. (104), and then post multiply by $\mathbf{C}_N^{-1}$, we obtain the following expression for the log-derivative matrix at $r = r_N$

$$\mathbf{Y}_N \cong \frac{1}{h}\left[\left(\frac{1}{2}\mathbf{I}-\mathbf{T}_{N+1}\right)\left(\mathbf{I}-\mathbf{T}_{N+1}\right)^{-1}\mathbf{R}_{N+1} - \left(\frac{1}{2}\mathbf{I}-\mathbf{T}_{N-1}\right)\left(\mathbf{I}-\mathbf{T}_{N-1}\right)^{-1}\mathbf{R}_N^{-1}\right]\left(\mathbf{I}-\mathbf{T}_N\right) \tag{105}$$

D. Operational outline of the renormalized Numerov method

Figure 14 shows the division of the r axis into N sectors, starting at $r = r_0$. Sector M is delimited by $r = r_{M-1}$ to the left and $r = r_M$ to the right. The renormalized Numerov

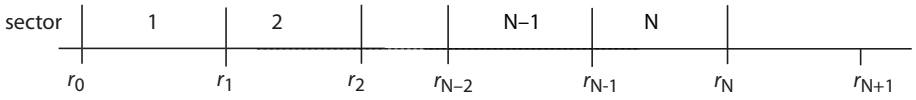

FIG. 14. Schematic partition of the r-axis into a series of sectors. The last sector ends at $r = r_N$. To determine the log-derivative matrix at $r = r_N$, we need to propagate one more step, out to $r = r_N + h$.

method proceeds by determining at the left-hand side of sector M, in order, $\mathbf{V}(r_{M-1})$, $\mathbf{W}(r_{M-1})$, $\mathbf{T}(r_{M-1})$ and $\mathbf{U}(r_{M-1})$, and then, with this information, transforming the ratio matrix at the left of sector M ($\mathbf{R}_{M-1}$) into the ratio matrix at the right of this same sector ($\mathbf{R}_M$). In this way the ratio matrix at $r = r_{M-1}$ is propagated to $r = r_M$.

At the end of the numerical propagation we have to carry out one more propagation step, out to $r = r_{N+1}$ (see Fig. 14). Then we use the ratio matrix at the right end-point of the last sector ($\mathbf{R}_N$), as well as the $\mathbf{T}$ matrices at $r = r_{N-1}$, $r = r_N$, and $r = r_{N+1}$ and the ratio matrix at the supplemental point $r = r_{N+1}$ to determine, by means of Eq. (105) the log-derivative matrix at $r = r_N$.

The operational outline of the renormalized Numerov propagation is as follows:

a. At the first integration point ($r = r_0$) determine $\mathbf{W}_0$ and then $\mathbf{T}_0 = -\frac{h^2}{12}\mathbf{W}_0$.

b. Determine $\mathbf{U}_0$ from Eq. (100) for $M = 0$.

c. Determine the ratio matrix $\mathbf{R}_1$ from Eq. (98). Also calculate the $\mathbf{T}$ matrix at the right-hand side of the first sector ($\mathbf{T}_1$).

Then repeat for $r = r_1 \to r_N$ (sectors 2, 3, ..., N) replacing steps $a - c$ with

b′. Determine $\mathbf{U}_{M-1}$ from Eq. (100)

c′. Determine the new ratio matrix $\mathbf{R}_M$ by use of Eq. (97), specifically $\mathbf{R}_M = \mathbf{U}_{M-1} - \mathbf{R}_{M-1}^{-1}$. Also calculate the $\mathbf{T}$ matrix at the right-hand side of the current sector ($\mathbf{T}_M$).

d. At the end of each sector, update the $\mathbf{T}$ and $\mathbf{R}$ matrices, namely

$$\mathbf{T}_{M-1} \to \mathbf{T}_{M-2} \qquad \mathbf{T}_M \to \mathbf{T}_{M-1} \qquad \mathbf{R}_M \to \mathbf{R}_{M-1}$$

e. Upon finishing the N^{th} sector, we carry out one more repetition of steps b' and c', out to $r_{N+1} = r_N + h$.

e. When propagation is completed, we have calculated $\mathbf{T}_{N-1}$, $\mathbf{T}_N$, $\mathbf{T}_{N+1}$ as well as $\mathbf{R}_N$, and, finally, $\mathbf{R}_{N+1}$. We use these matrices to determine, from Eq. (105), the log-derivative matrix at $r = r_N$ ($\mathbf{Y}_N$).

E. Determination of the S matrix

We know from Eq. (86) that

$$\lim_{r\to\infty} \mathbf{C}(r) = \hat{\mathbf{h}}^{(2)}(r) - \hat{\mathbf{h}}^{(1)}(r)\mathbf{S} \tag{106}$$

Differentiation gives

$$\lim_{r\to\infty} \mathbf{C}(r)' = \hat{\mathbf{h}}^{(2)}(r)' - \hat{\mathbf{h}}^{(1)}(r)'\mathbf{S} \tag{107}$$

where $\hat{\mathbf{h}}^{(1,2)}(r)'$ are diagonal matrices, with elements given by the derivatives of the diagonal elements in Eq. (85). From the preceding two equations, we see that

$$\lim_{r\to\infty} \mathbf{Y}(r) = \mathbf{Y}(r_N) = \mathbf{Y}_N = \left[\hat{\mathbf{h}}^{(2)}(r_N)' - \hat{\mathbf{h}}^{(1)}(r_N)'\mathbf{S}\right]\left[\hat{\mathbf{h}}^{(2)}(r_N) - \hat{\mathbf{h}}^{(1)}(r_N)\mathbf{S}\right]^{-1} \tag{108}$$

This equation can be rearranged to yield

$$\left[\hat{\mathbf{h}}^{(1)}(r_N)' - \mathbf{Y}(r_N)\hat{\mathbf{h}}^{(1)}(r_N)\right]\mathbf{S} = \left[\hat{\mathbf{h}}^{(2)}(r_N)' - \mathbf{Y}(r_N)\hat{\mathbf{h}}^{(2)}(r_N)\right] \tag{109}$$

Since we have previously determined $\mathbf{Y}(r_N)$, we can solve this set of complex linear equations for the S matrix. Alternatively, the linear equations can be decomposed into real and imaginary parts, which you can solve using real (rather than complex) arithmetic for the real and imaginary parts of $\mathbf{S}$.

If the angular momentum l is zero, then the elements of the diagonal $\hat{\mathbf{h}}^{(1,2)}(r)$ matrices are

$$\hat{h}^{(1,2)}_{nn}(r) = (\mp i)k_n^{-1/2}\exp(\pm i k_n r) \tag{110}$$

where the upper sign goes with the $\hat{\mathbf{h}}^{(1)}$ matrix [see Eq. (87)].

Problem 21

Demonstrate the expansion of the wavefunction of Eq. (78) reduces the Schrodinger equation (76) to the set of coupled ordinary differential equations of Eq. (79).

Problem 22

Show that introduction of the ratio matrix [Eq. (96)] allows you to transform the matrix Numerov equation (94) into the matrix equation for $\mathbf{R}$, namely Eq. (97).

Problem 23

Demonstrate that Eq. (102) follows from subtraction of the two equations which precede it.

Problem 24

Show how the overall propagation equation in the renormalized Numerov method (101) follows from the equations which precede it.

Problem 25

Show how Eq. (109) follows from Eq. (108).

Problem 26

Immediately after Eq. (109) we mention that you can obtain the real and imaginary parts of **S** separately, by solution of two sets of linear equations each of which involve only real quantities. Derive these equations.

F. Illustrative calculation: Asymptotic basis

Consider two coupled equations, which represent the coupling between the $^2P_{1/2}$ and $^2P_{3/2}$ states of the Cl atom, both with $\Omega = 1/2$, induced by collisions with a spherical H_2 molecule. The matrix of the potential is

$$\mathbf{V}(r) = \begin{bmatrix} \frac{2}{3}V_\Sigma + \frac{1}{3}V_\Pi - A & \frac{\sqrt{2}}{3}(V_\Pi - V_\Sigma) \\ \frac{\sqrt{2}}{3}(V_\Pi - V_\Sigma) & \frac{1}{3}V_\Sigma + \frac{2}{3}V_\Pi + 2A \end{bmatrix} \tag{111}$$

where the spin-orbit constant is $A = 293.3$ cm^{-1}. The potentials V_Π and V_Σ are fit by the functional form

$$V_{\Sigma(\Pi)}(r) = C_1 e^{-\lambda_1 r} + (C_2 + C_3 r)\, e^{-\lambda_2 r} - \frac{C_4}{2}\left\{\tanh\left[1.2\,(r - \lambda_3)\right] + 1\right\} r^{-6}$$

The constants (energies in cm^{-1} and distances in a_0) are given in Tab. VI.

TABLE VI. Constants defining two-state inelastic scattering model[a]

	V_Σ	V_Π
λ_1	0.813	0.677
λ_2	1.2014	2.2061
λ_3	5.5701	6.2093
C_1	3.7457(+3)	–7.7718(+3)
C_2	6.7280(+5)	–7.3837(+7)
C_3	–1.2773(+5)	3.2149(+7)
C_4	3.4733(+6)	2.9743(+6)

[a] Powers of ten in parentheses

Plot the dependence on r of the matrix elements in Eq. (111) and, with dashed lines on the same plot, the dependence on r of the two eigenvalues which you obtain by diagonalizing the 2×2 matrix of Eq. (111).

Let the reduced mass be 2.85 atomic mass units and the angular momentum $l = 0$. It is most convenient to work in Hartree atomic units, in which $\hbar = 1$. (1 cm^{-1} = 219474.6 Hartree, and 1 amu = 1822.889 atomic units) Write a Matlab script or Fortan code to calculate the inelastic transition probability, $|S_{12}|^2$, at energies of 600, 800, 1000, 1500, and 2000 cm^{-1}. This is the probability that an atom in the upper (or lower) spin-orbit state will be transferred by collision to the other spin-orbit state. To check that your code is working, for $E = 1000$ cm^{-1}, $r_0 = 3.5$ a_0, $N = 200$, $r_N = 22$ a_0, you should obtain

$$\mathbf{Y}_N \equiv \mathbf{Y}(r = r_N) = \begin{bmatrix} 37.384 & -0.72415 \\ -0.72528 & -3.9881 \end{bmatrix}$$

and

$$\mathbf{S} = \begin{bmatrix} 0.11949 - 0.99213i & -0.0025682 + 0.037300i \\ -0.0025723 + 0.037358i & -0.017617 + 0.99914i \end{bmatrix} \tag{112}$$

The S matrix should be symmetric (which is a consequence of time-reversibility). The result shown above is not quite symmetric. This is a consequence of the error introduced by discretization. Increasing the number of sectors results in convergence to a fully symmetric matrix. This is shown by the results in the Tab. VII.

TABLE VII. Convergence of inelastic components of the S matrix for the model two-channel inelastic scattering illustration.

N	$(S_{12} + S_{21})/2$	$(S_{12} - S_{21})/2$
100	–0.03305+0.0033661i	3.2306×10^{-4}–$3.2903\times10^{-5}\,i$
200	–0.0025703+0.037329i	2.007×10^{-6}–$2.9151\times10^{-5}\,i$
300	–0.0000095+0.037501i	1.534×10^{-9}–$6.0816\times10^{-6}\,i$
500	0.00053111+0.037514i	-1.146×10^{-8}–$8.0943\times10^{-7}\,i$
1000	0.00060658+0.037515i	-8.273×10^{-10}–$5.1162\times10^{-8}\,i$

Another check is that the sum of the absolute value squared of any column of the S matrix should add to unity (which is a consequence of conservation of probability).

Figure 15 on the next page shows the convergence of the inelastic transition probabilities (the absolute value squared of the off-diagonal elements of the S matrix) as the number of sectors is increased. For an energy of 1000 cm^{-1} and a reduced mass of 2.85 atomic mass units the de Broglie wavelength is ≈ 0.91 a_o. Typically, you need the sector size to be $\approx$1/10

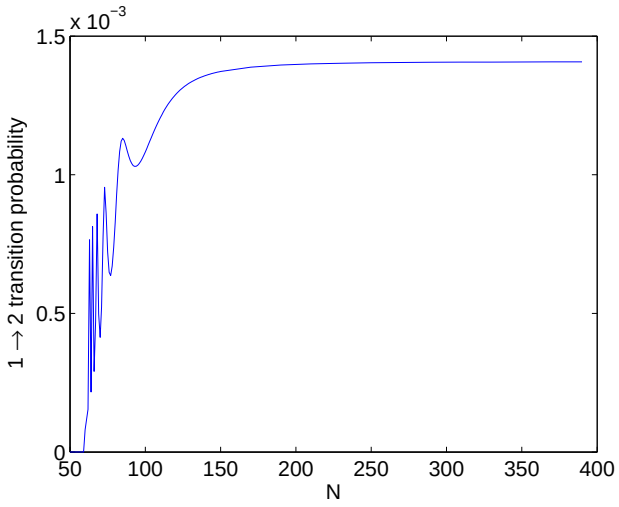

FIG. 15. Convergence of the inelastic transition probability for the model two-channel inelastic scattering illustration.

the deBroglie wavelength for the numerical integration to be accurate. Here that translates to a sector size of $\approx 0.09\ a_o$, or ≈ 200 sectors to cover the range $3.5 \leq r \leq 22$. We see from Fig. 15 that even with ≈ 150 sectors the calculated inelastic probabilities have converged to within 1 %.

G. Using the renormalized Numerov method in the locally adiabatic basis

An alternative solution scheme involves propagating in a locally adiabatic basis (see also Ref. [14]). We refer the reader back to Fig. 14 on page 44. Let $\mathbf{V}_M$ be the matrix of the potential [Eq. (80)] at $r = r_M$, namely $\mathbf{V}_M \equiv \mathbf{V}(r_M)$. Then, let $\mathbf{X}_M$ be the matrix which diagonalizes $\mathbf{V}_M$, namely

$$\mathbf{X}_M^T\, \mathbf{V}(r_M)\, \mathbf{X}_M = \mathbf{X}_M^T\, \mathbf{V}_M\, \mathbf{X}_M = \tilde{\mathbf{v}}_M \tag{113}$$

where $\tilde{\mathbf{v}}_M$ is the diagonal matrix of the eigenvalues. Since the matrix of the potential is either symmetric (or Hermitian), the matrix $\mathbf{X}$ will define an orthogonal (or unitary) transformation. We shall assume that $\mathbf{V}$ is a real, symmetric matrix. Hereafter, we use the superscript tilde to designate quantities in the locally adiabatic basis. The columns of the matrix $\mathbf{X}_M$ are the linear combinations of the functions $\{\chi(q)\}$ in which the matrix of

$H(r,q)$ is diagonal at $r = r_M$. We will designate these functions $\{\phi_M(q)\}$, so that

$$\{\phi_M\} = \mathbf{X}_M^T \{\chi\}$$

Here, both $\{\phi_M(q)\}$ and $\{\chi(q)\}$ are column vectors.

The goal is to obtain the matrix $\mathbf{C}(r)$ which is a set of linearly-independent combinations of the internal states $\{\chi(q)\}$ which solve Eq. (81). The renormalized Numerov method works by propagating the ratio matrix which [as seen in Eq. (96)] is related to a product of the solution matrix $\mathbf{C}$ at one point and the inverse of the solution matrix at the previous point.

Now, suppose we chose to propagate the solution in the locally adiabatic basis. In this approach we will seek, in each sector, the matrix $\tilde{\mathbf{C}}_M(r)$ which is the set of linearly-independent combinations of the *locally adiabatic* states $\{\phi_M\}$ which are solutions to the CC equations. For simplicity, we shall suppress the variable q unless needed. In the preceding sections, we considered solution of the close-coupled equations in the asymptotic basis $\{\chi\}$.

Obviously, the $\tilde{\mathbf{C}}_M(r)$ matrix is related to the $\mathbf{C}_M(r)$ matrix by the transformation $\mathbf{X}_M$. The application of the renormalized Numerov method in the locally-adiabatic basis will require first working through the algebra associated with propagating the ratio matrix in the locally-adiabatic basis. At first thought this seems like a more cumbersome way to solve the equations, especially since matrix diagonalization is required at each additional grid point. However, it will offer some advantages, particularly if one is interested in determining cross sections for scattering at a large number of collision energies or if one has access to computational hardware and vector libraries which permit a high degree of parallelization.

Propagation in the locally adiabatic basis will make use of the locally-adiabatic equivalent of the $\mathbf{F}_M$ matrix of Eq. (93), which we will designate by the superscript tilde, namely

$$\tilde{\mathbf{F}}_M = \left(\mathbf{I} - \tilde{\mathbf{T}}_M\right) \tilde{\mathbf{C}}_M \tag{114}$$

where

$$\tilde{\mathbf{T}}_M = \mathbf{X}_M^T \mathbf{T}_M \mathbf{X}_M \tag{115}$$

Now, since $\tilde{\mathbf{C}}_M = \mathbf{X}_M^T \mathbf{C}_M$ and since $\mathbf{I} = \mathbf{X}_M^T\, \mathbf{I}\, \mathbf{X}_M$, we can rearrange Eq. (114) as

$$\tilde{\mathbf{F}}_M = \left(\mathbf{I} - \tilde{\mathbf{T}}_M\right) \tilde{\mathbf{C}}_M = \mathbf{X}_M^T \left(\mathbf{I} - \mathbf{T}_M\right) \mathbf{X}_M \tilde{\mathbf{C}}_M = \mathbf{X}_M^T \left(\mathbf{I} - \mathbf{T}_M\right) \mathbf{C}_M \tag{116}$$

Comparing the right-hand side with Eq. (93), we conclude that

$$\tilde{\mathbf{F}}_M = \mathbf{X}_M^T \mathbf{F}_M \tag{117}$$

This demonstrates that the $\mathbf{F}$ matrix transforms as the basis functions. This is reasonable, since [Eq. (114)] reveals that $\tilde{\mathbf{F}}$ is just a linear combination of the solutions $\tilde{\mathbf{C}}$.

The Numerov propagation relation in the asymptotic basis is given by Eq. (94), which we repeat here:

$$\mathbf{F}_{M+1} - \mathbf{U}_M \mathbf{F}_M + \mathbf{F}_{M-1} = 0 \tag{118}$$

Using Eq. (117) to transform the three $\mathbf{F}$ matrices into the locally adiabatic basis, we find

$$\mathbf{X}_{M+1}\tilde{\mathbf{F}}_{M+1} = \mathbf{U}_M \mathbf{X}_M \tilde{\mathbf{F}}_M - \mathbf{X}_{M-1}\tilde{\mathbf{F}}_{M-1} \tag{119}$$

We then postmultiply by $\tilde{\mathbf{F}}_M^{-1}$ and premultiply by $\mathbf{X}_M^T$ to get

$$\mathbf{X}_M^T \mathbf{X}_{M+1}\tilde{\mathbf{F}}_{M+1}\tilde{\mathbf{F}}_M^{-1} = \mathbf{X}_M^T \mathbf{U}_M \mathbf{X}_M - \mathbf{X}_M^T \mathbf{X}_{M-1}\tilde{\mathbf{F}}_{M-1}\tilde{\mathbf{F}}_M^{-1} \tag{120}$$

Now, the overlap between the locally-adiabatic functions in sector M and those in sector $M+1$ is

$$\mathbf{O}_{M,M+1} = \mathbf{X}_M^T \mathbf{X}_{M+1} \tag{121}$$

so that the preceding equation can be written as

$$\mathbf{O}_{M,M+1}\tilde{\mathbf{F}}_{M+1}\tilde{\mathbf{F}}_M^{-1} = \mathbf{X}_M^T \mathbf{U}_M \mathbf{X}_M - \mathbf{O}_{M-1,M}^T \tilde{\mathbf{F}}_{M-1}\tilde{\mathbf{F}}_M^{-1} \tag{122}$$

If we define the ratio matrix in the locally-adiabatic basis as

$$\tilde{\mathbf{R}}_M \equiv \mathbf{O}_{M-1,M}\tilde{\mathbf{F}}_M\tilde{\mathbf{F}}_{M-1}^{-1} \tag{123}$$

then Eq. (122) becomes

$$\tilde{\mathbf{R}}_{M+1} = \mathbf{X}_M^T \mathbf{U}_M \mathbf{X}_M - \mathbf{O}_{M-1,M}^T \tilde{\mathbf{R}}_M^{-1} \mathbf{O}_{M-1,M}$$

$$= \tilde{\mathbf{U}}_M - \mathbf{O}^T_{M-1,M}\tilde{\mathbf{R}}^{-1}_M\mathbf{O}_{M-1,M} \tag{124}$$

where $\tilde{\mathbf{U}}_M$ is the transform of the $\mathbf{U}_M$ matrix into the locally adiabatic basis. Now, we remember that

$$\mathbf{U}_M = (2\mathbf{I} + 10\mathbf{T}_M)(\mathbf{I} - \mathbf{T}_M)^{-1}$$

Premultiplying by $\mathbf{X}^T_M$, postmultiplying by $\mathbf{X}_M$, and inserting a factor of $\mathbf{I} = \mathbf{X}_M\mathbf{X}^T_M$ immediately after the term $(2\mathbf{I} + 10\mathbf{T}_M)$ gives

$$\begin{aligned}\mathbf{X}^T_M\mathbf{U}_M\mathbf{X}^M &= \mathbf{X}^T_M(2\mathbf{I} + 10\mathbf{T}_M)\mathbf{X}_M\mathbf{X}^T_M(\mathbf{I} - \mathbf{T}_M)^{-1}\mathbf{X}_M \\ &= \mathbf{X}^T_M(2\mathbf{I} + 10\mathbf{T}_M)\mathbf{X}_M\left[\mathbf{X}^T_M(\mathbf{I} - \mathbf{T}_M)\mathbf{X}_M\right]^{-1}\end{aligned} \tag{125}$$

We recall that the $\mathbf{T}$ matrix is defined by Eq. (92). Since the $\mathbf{V}$ matrix is diagonalized by the $\mathbf{X}$ matrix, it follows that the $\mathbf{T}$ matrix is also diagonalized, with elements

$$\left(\tilde{\mathbf{T}}_\mathbf{M}\right)_{nn} = -\frac{h^2}{12}2\mu\left[E - \tilde{\mathbf{v}}_n(r = r_M)\right] \tag{126}$$

Consequently, we conclude from Eq. (125) that the $\tilde{\mathbf{U}}_M$ matrix is also diagonal, namely

$$\mathbf{X}^T_M\mathbf{U}_M\mathbf{X}_M = \tilde{\mathbf{u}}_M$$

with elements

$$(\tilde{\mathbf{u}}_\mathbf{M})_{nn} = \left[2 + 10\left(\tilde{\mathbf{t}}_\mathbf{M}\right)_{nn}\right]\Big/\left[1 - \left(\tilde{\mathbf{t}}_\mathbf{M}\right)_{nn}\right] \tag{127}$$

Consequently, Eq. (124) becomes (see Ref. [11] for an alternate explanation of this entire derivation)

$$\tilde{\mathbf{R}}_{M+1} = \tilde{\mathbf{u}}_M - \mathbf{O}^T_{M-1,M}\tilde{\mathbf{R}}^{-1}_M\mathbf{O}_{M-1,M} \tag{128}$$

Suppose we are interested in running scattering calculations at multiple energies. The transformation matrices $\mathbf{X}_M$ and, thus, $\mathbf{O}_{M-1,M}$ are independent of energy. Thus the $\tilde{\mathbf{O}}_{M-1,M}$ matrices need only be computed once. Once the $\mathbf{O}$ matrices are computed and stored, the propagation of Eq. (128) involves just a linear equation solution followed by a matrix multiply to propagate the ratio matrix from one sector to the next. This is particularly efficient if one wants solutions at a lot of energies. The detailed algorithm is as follows:

1. Solve a set of simultaneous linear equations for the (temporary) matrix $\mathbf{B}$, namely

$$\tilde{\mathbf{R}}_M \mathbf{B}_M = \mathbf{O}_{M-1,M}$$

2. Obtain $\tilde{\mathbf{R}}_{M+1}$ from $\mathbf{B}$ as

$$\tilde{\mathbf{R}}_{M+1} = \tilde{\mathbf{u}}_M - \mathbf{O}^T_{M-1,M} \mathbf{B}_M$$

Typically one would use the Lapack routines `DGESV` for step 1 and `DGEMM` for step 2. In the solution of the matrix equations $\mathbf{AB} = \mathbf{C}$, the routine `DGESV` overwrites both $\mathbf{A}$ and $\mathbf{C}$. Thus, it will be necessary to store $\mathbf{O}_{M-1,M}$, obtain $\mathbf{B}$, then used the stored matrix $\mathbf{O}_{M-1,M}$ to obtain $\mathbf{O}^T_{M-1,M}\mathbf{B}$.

Propagation in the locally-adiabatic basis produces the ratio matrices in the locally-adiabatic basis. It is easy to show using Eqs. (117) and (121) that

$$\begin{aligned} \tilde{\mathbf{R}}_M &\equiv \mathbf{O}_{M-1,M} \tilde{\mathbf{F}}_M \tilde{\mathbf{F}}^{-1}_{M-1} \\ &= \mathbf{X}^T_{M-1} \mathbf{F}_M \mathbf{F}^{-1}_{M-1} \mathbf{X}_{M-1} = \mathbf{X}^T_{M-1} \mathbf{R}_M \mathbf{X}_{M-1} \end{aligned} \tag{129}$$

Reversing the transformation gives

$$\mathbf{R}_M = \mathbf{X}_{M-1} \tilde{\mathbf{R}}_M \mathbf{X}^T_{M-1} \tag{130}$$

so that the ratio matrix in the asymptotic basis is the inverse transform of the ratio matrix in the locally-adiabatic basis.

H. Determination of the log-derivative matrix in the asymptotic basis

We know from Sec. V E that the S matrix can be determined from a knowledge of the log-derivative matrix at $r = r_N$. In the asymptotic basis, Eq. (105) gives the relation between $\mathbf{Y}_N$ and the $\mathbf{T}$ and $\mathbf{R}$ matrices at points $N-1$, N, and $N+1$. Making use of Eqs. (115) and (129), we can rewrite Eq. (105) as

$$\mathbf{Y}_N \cong \frac{1}{h} \left[\mathbf{X}_{N+1} \left(\frac{1}{2}\mathbf{I} - \tilde{\mathbf{T}}_{N+1} \right) \left(\mathbf{I} - \tilde{\mathbf{T}}_{N+1} \right)^{-1} \mathbf{O}^T_{N,N+1} \tilde{\mathbf{R}}_{N+1} \right.$$

$$-\mathbf{X}_{N-1}\left(\frac{1}{2}\mathbf{I}-\tilde{\mathbf{T}}_{N-1}\right)\left(\mathbf{I}-\tilde{\mathbf{T}}_{N-1}\right)^{-1}\tilde{\mathbf{R}}_N^{-1}\mathbf{O}_{N-1,N}\Big]\left(\mathbf{I}-\tilde{\mathbf{T}}_N\right)\mathbf{X}_N^T \tag{131}$$

Problem 27

Carry out the algebra leading from Eqs. (117) and (121) to Eq. (129). Then, make use of Eqs. (115) and (129) to transform Eq. (105) into Eq. (131).

I. Initialization and propagation algorithm: locally-adiabatic basis

How is the renormalized Numerov propagator in the locally-adiabatic basis initialized? In

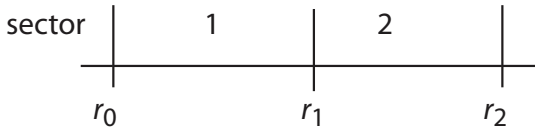

FIG. 16. Initial sectors

the initial sector we diagonalize the $\mathbf{V}(r)$ matrix at $r = r_0$. The diagonalizing transformation is $\mathbf{X}_0$. We then initiate propagation in the locally adiabatic basis using Eq. (98), namely

$$\tilde{\mathbf{R}}_1 = \tilde{\mathbf{u}}_0 \tag{132}$$

where $\tilde{\mathbf{u}}_0$ is given by [see Eq. (127)]

$$(\tilde{\mathbf{u}}_0)_n = \left[2 + 10\left(\tilde{\mathbf{t}}_0\right)_n\right] \Big/ \left[1 - \left(\tilde{\mathbf{t}}_0\right)_n\right] \tag{133}$$

At the right hand side of the first sector (at $r = r_1$), we obtain the next diagonalizing transform $\mathbf{X}_1$ and then the first overlap matrix [Eq. (121)]

$$\mathbf{O}_{0,1} = \mathbf{X}_0^T \mathbf{X}_1$$

The locally-adiabatic matrix at $r = r_1$ is then obtained from Eq. (128) as

$$\tilde{\mathbf{R}}_2 = \tilde{\mathbf{u}}_1 - \mathbf{O}_{0,1}^T \tilde{\mathbf{R}}_1^{-1} \mathbf{O}_{0,1}$$

The operational outline of the renormalized Numerov propagation in the locally adiabatic basis is as follows (let M be the sector index, ranging from $M = 1$ to $M = N$.

a. At the first integration point ($r = r_0$) determine $\mathbf{V}_0$. Diagonalize $\mathbf{V}_0$ to obtain $\mathbf{X}_0$. Call this `XMm1`.

b. Determine $\tilde{\mathbf{T}}_0$ and $\tilde{\mathbf{u}}_0$ from Eqs. (126) and (127) for $M = 0$. Call these `ttMm1` and `uMm1`.

c. Determine the ratio matrix $\tilde{\mathbf{R}}_1$ from Eq. (132). Call this `RtM`.

d. Determine $\mathbf{V}$ at the right-hand-side of the sector ($r = r_M$). Diagonalize this matrix to obtain $\mathbf{X}_M$. Call this `XM`. From this, and the matrix $\mathbf{X}_{M-1}$, which you have already calculated (see step *a* above), obtain the overlap matrix $\mathbf{O}_{M-1,M} = \mathbf{X}_{M-1}^T \mathbf{X}_M$. Call this `OMm1M`.

e. From $\mathbf{V}(r_M)$ and $\mathbf{X}_M$ Determine $\tilde{\mathbf{T}}$ and $\tilde{\mathbf{u}}$ at the right-hand-side of the sector. Call these `ttM` and `uM`.

f. **Except** for the last sector, update the $\tilde{\mathbf{T}}$, $\tilde{\mathbf{u}}$, $\mathbf{X}$, $\tilde{\mathbf{R}}$, and $\tilde{\mathbf{O}}$ matrices, namely

`ttMm1` → `ttMm2` `ttMm` → `ttMm1` `XMm1` → `XMm2` `XM` → `XMm1` `RtM` → `RtMm1` `uMm` → `uMm1` `OMm1M` → `OM`

Then repeat steps $c - f$ for sectors 2, 3, ..., $N + 1$, replacing step *c* with

c′. From $\tilde{\mathbf{u}}_{M-1}$ and $\mathbf{O}_{M-2,M-1}$ (which you have already calculated as `uMm1` and `OMm2Mm1`), determine the ratio matrix $\tilde{\mathbf{R}}_M$ from Eq. (128).

g. Upon finishing the N^{th} sector, we carry out one more repetition out to $r_{N+1} = r_N + h$, **without** the update step *f* .

When propagation is completed, we have calculated $\tilde{\mathbf{T}}_{N-1}$, $\tilde{\mathbf{T}}_N$, $\tilde{\mathbf{T}}_{N+1}$, $\mathbf{X}_{N-1}$, $\mathbf{X}_N$, $\mathbf{X}_{N+1}$ as well as $\tilde{\mathbf{R}}_N$, and, finally, $\tilde{\mathbf{R}}_{N+1}$. We use these matrices to determine, from Eq. (131), the log-derivative matrix at $r = r_N$ ($\mathbf{Y}_N$). Determination of the S-matrix is done according to Sec. V E, identical to when propagation is carried out in the asymptotic basis.

J. Illustrative calculation

Carry out the sample two-state calculation of Sec. V F in the locally adiabatic treatment. I would encourage you to write your own Matlab script, but, just in case you're lazy, you can get a copy of the script here. You should get exactly the same results as in the calculation using the asymptotic basis. In fact, for the illustrative calculation done in Sec. V F you should obtain

$$\mathbf{S} = \begin{bmatrix} 0.11959 - 0.99213i & -0.0025682 + 0.037299i \\ -0.0025777 + 0.037358i & -0.017805 + 0.99914i \end{bmatrix} \tag{134}$$

Which differs insignificantly from Eq. (112). Table VII, which compares the symmetry of the calculated inelastic S-matrix elements as a function of the number of steps, becomes replaced here by

TABLE VIII. Convergence of inelastic components of the S matrix for the model two-channel inelastic scattering illustration. Propagation in the locally adiabatic basis.[a]

N	$(S_{12} + S_{21})/2$	$(S_{12} - S_{21})/2$
100	–0.03305+0.0033566i	3.2306×10^{-4}–3.2903×10^{-5} i
200	–0.0025703+0.037329i	2.007×10^{-6}–2.9151×10^{-5} i
300	–0.00001311+0.037501i	1.534×10^{-9}–6.0816×10^{-6} i
500	0.00052891+0.037514i	–1.146×10^{-8}–8.0943×10^{-7} i
1000	0.00060658+0.037515i	–8.273×10^{-10}–5.1162×10^{-8} i

[a] The differences with Tab. VII are given in red.

K. Enhanced Numerov propagator

The conventional Numerov propagator, in either the original or renormalized versions, is based on Eq. (94). For a set of uncoupled equations, as we have in each locally-adiabatic sector, the $\mathbf{U}$ matrix is diagonal with elements defined by Eq. (127). Thorlacius and Cooper [15] suggest a slightly different propagator, in which all elements of the diagonal $\tilde{\mathbf{u}}_M$ matrix given in Eq. (127) for which $\tilde{T}_{nn} < 0$ are replaced by

$$(\tilde{\mathbf{u}}_M)_n = 2\cos\left[\left(-12\tilde{T}_{nn}\right)^{1/2}\right].$$

This modification is called the "enhanced Numerov algorithm". Figure 17 compares the inelastic transition probabilities and the relative fractional error in the inelastic transition probability for the two-channel problem of Sec. V F, as computed by the Renormalized Numerov method in the asymptotic basis and by the enhanced Numerov method in the locally adiabatic basis. We see that although at low energy both methods, and, in particular,

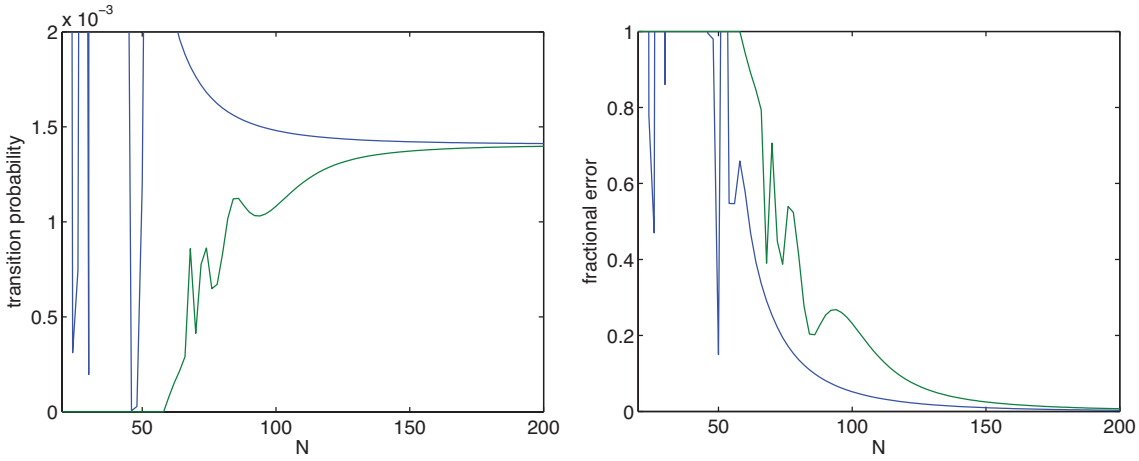

FIG. 17. Comparison of calculated transition probabilities (left panel) and relative fractional error (right panel) for the two-state problem of Sec. V F. The blue and green curves correspond, respectively, to using enhanced renormalized Numerov propagation in the locally-adiabatic basis and conventional renormalized Numerov propagation in the asymptotic basis

the enhanced renormalized version fails miserably. However, for $N \simeq 75$, the enhanced renormalized Numerov method is dramatically more accurate.

L. Advantages of the locally-adiabatic propagation

Solution of the close-coupled equations in the asymptotic basis requires two matrix inversions per sector. The operational count for this is $8n^3/3$ where n is the number of coupled equations. Solution of the close-coupled equations in the locally-adiabatic basis requires solution of a full (n right-hand-sides) set of linear equations followed by a matrix multiply. The operational count is $4n^3/3 + n^3 = 7n^3/3$, slightly less. However, to determine the locally-adiabatic basis requires one matrix diagonalization per sector, as well as a matrix multiply to determine the overlap matrix $\mathbf{O}_{N-1,N}$, roughly $11n^3/3$ operations

Thus, for solution of the close-coupled equations at a single collision energy, the asymptotically-based method is to be preferred. However, if one is interested in solutions at m collision

energies. The operational count will be $8mn^3/3$ for the asymptotically-based method. Since the diagonalization is independent of the collision energy, since the potential matrix $\mathbf{V}(\mathrm{r})$ is unchanged, this operation, and the determination of the overlap matrix, need be done only once. Consequently, the operational count for the locally-adiabatic method will be $(7m + 11)n^3/3$ operations. This will become competitive for $m > 11$.

Also, since matrix multiplication will benefit the most (or the easiest) from parallelization, in a parallel environment the locally-adiabatic method, which involves one matrix multiply and one solution of a set of linear equations, may be practically more efficient than the asymptotically-based method, which involves two matrix inversions.

In addition, in the locally-adiabatic method one can exploit the Thorlacius-Cooper enhanced propagator to gain a sufficient degree of accuracy with fewer sectors.

VI. ROTATIONALLY INELASTIC SCATTERING

Here we will adapt the general discussion of inelastic scattering from the previous section to the particular case of collisions of a rigid rotor with a closed-shell, spherical partner. The states of the rigid-rotor target will the labelled with the space-frame quantum numbers j and m with energy ε_j (independent of m_j) and coordinate representation

$$|jm_j\rangle \equiv Y_{jm_j}(\hat{r})$$

where $\hat{r}$ is the orientation of the molecular axis. Asymptotically, the wave function for the scattering system describes an incoming plane wave with the molecule in rotational state $|jm_j\rangle$ and a scattered wave including a contribution from all energetically accessible rotational states, namely

$$\lim_{R\to\infty} \Psi^{(jm_j)}(\vec{R},\hat{r}) = e^{ik_j Z}\,|jm_j\rangle + \sum_{j'm_{j'}} \frac{1}{\sqrt{k_j k_{j'}}} f_{jm_j\to j'm_{j'}}(\hat{R})\,|j'm_{j'}\rangle\,\frac{e^{ik_{j'}R}}{R} \tag{135}$$

where the wave vectors are (in atomic units) $k_j = [2\mu(E - \varepsilon_j)]^{1/2}$. Here upper-case R designates the atom-molecule separation coordinate, while $\vec{r}$ which designates the orientation of the bond axis of the diatomic. Note that the elastic term ($j' = j$ and $m_{j'} = m_j$) reduces to Eq. (60) which we derived in the section on quantum elastic scattering

Following the analysis of the scattering wave function in the Section on Elastic Scattering (see **??**), the ratio of the outgoing flux per unit solid angle in state $|j'm_{j'}\rangle$ to the incoming flux per unit area in $|jm_j\rangle$ is $|f_{jm_j\to j'm_{j'}}|^2/k_j^2$. This quantity has the dimensions of area and is the differential cross section associated with the transition $jm_j \to j'm_{j'}$.

A. Partial Wave Decomposition

We can easily extend Eq. (68) to the inelastic case, (but here using upper-case R to designate the atom-molecular separation coordinate) writing

$$\lim_{r\to\infty}\Psi(\vec{R},\hat{r}) = \sum_l (2l+1)\left[\frac{i}{2}\sum_{j'm_{j'}} f^{(l)}_{jm_j\to j'm_{j'}}\frac{e^{ik_{j'}R}}{k_{j'}R}\,|j'm_{j'}\rangle + i^l j_l(kR)\,|jm_j\rangle\right] P_l(\cos\theta) \quad (136)$$

where we have followed Eq. (66) in expanding the elastic and inelastic scattering amplitudes in Legendre polynomials, namely

$$f_{jm_j\to j'm_{j'}}(\hat{R}) = \sum_l \frac{1}{2}(2l+1) f^{(l)}_{jm_j\to j'm_{j'}} P_l(\cos\theta) = i\sum_l \frac{1}{2i}(2l+1) f^{(l)}_{jm_j\to j'm_{j'}} P_l(\cos\theta) \quad (137)$$

The scattering will be azimuthally symmetric, so that the results will depend only on the polar angle θ. Note that we are using upper-case R to designate the atom-molecule separation coordinate, as opposed to $\vec{r}$ which designates the bond axis of the diatomic.

VII. COLLINEAR REACTIVE SCATTERING

A. Bond, Jacobi, and mass-scaled Jacobi coordinates

Consider the collinear reaction A+BC→AB+C. Let x_i (where $i = a, b, c$) designate the position of each atom. The kinetic energy operator is

$$\hat{T} = -\frac{1}{2m_a}\frac{d^2}{dx_a^2} - \frac{1}{2m_b}\frac{d^2}{dx_b^2} - \frac{1}{2m_c}\frac{d^2}{dx_c^2} \quad (138)$$

Define three new coordinates (which we shall designate collectively **q**), namely the position of the center-of-mass

$$R = \frac{m_a x_a + m_b x_b + m_c x_c}{M}$$

where $M = m_a + m_b + m_c$, as well as the two bond distances

$$u_1 = x_b - x_a$$

and

$$u_2 = x_c - x_b$$

Problem #21 Using the chain rule

$$\frac{d}{dx_a} = \frac{d}{du_1}\frac{du_1}{dx_a} + \frac{d}{du_1}\frac{du_1}{dx_b} + \frac{d}{dR}\frac{dR}{dx_a}$$

(and, similarly, for dx/dx_b and d/dx_c) show that the second derivatives which enter into Eq. (138) are given by

$$\frac{d^2}{dx_a^2} = \frac{d^2}{du_1^2} - \frac{2m_a}{M}\frac{d^2}{du_1 dR} + \frac{m_a^2}{M^2}\frac{d^2}{dR^2}$$

$$\frac{d^2}{dx_b^2} = \frac{d^2}{du_1^2} - 2\frac{d^2}{du_1 du_2} + \frac{d^2}{du_2^2} - \frac{2m_b}{M}\frac{d^2}{du_1 dR} - \frac{2m_b}{M}\frac{d^2}{du_2 dR} + \frac{m_b^2}{M^2}\frac{d^2}{dR^2}$$

and

$$\frac{d^2}{dx_c^2} = \frac{d^2}{du_2^2} - \frac{2m_c}{M}\frac{d^2}{du_2 dR} + \frac{m_c^2}{M^2}\frac{d^2}{dR^2}$$

Consequently, in terms of the variables u_1, u_2 and R the kinetic energy operator is

$$\hat{T} = -\frac{1}{2}\left[\frac{1}{M}\frac{d^2}{dR^2} + \frac{1}{\mu_{ab}}\frac{d^2}{du_1^2} + \frac{1}{\mu_{bc}}\frac{d^2}{du_2^2} - \frac{2}{m_b}\frac{d^2}{du_1 du_2}\right]$$

where μ_{ab} is the AB reduced mass

$$\mu_{ab} = \frac{m_a m_b}{m_a + m_b}$$

and similarly for μ_{bc}.

If we define the row vector

$$\frac{\mathbf{d}}{\mathbf{du}} = \left[\frac{d}{du_1}\ \frac{d}{du_2}\ \frac{d}{dR}\right]$$

Then we can rewrite the kinetic energy operator in matrix form

$$\hat{\mathbf{T}}_q = \frac{1}{2}\frac{\mathbf{d}}{\mathbf{du}}\,\boldsymbol{\mu}_q^{-1}\,\frac{\mathbf{d}}{\mathbf{du}}^T \tag{139}$$

where

$$\boldsymbol{\mu}_q = \frac{1}{M}\begin{bmatrix} m_a(m_b+m_c) & m_a m_c & 0 \\ m_a m_c & m_c(m_a+m_b) & 0 \\ 0 & 0 & M^2 \end{bmatrix}$$

and

$$\boldsymbol{\mu}_q^{-1} = \frac{1}{M}\begin{bmatrix} \mu_{ab}^{-1} & -1/m_b & 0 \\ -1/m_b & \mu_{bc}^{-1} & 0 \\ 0 & 0 & 1 \end{bmatrix}$$

Here μ_{ab} and μ_{bc} are the usual AB and BC reduced masses, namely $\mu_{ab} = m_a m_b/(m_a+m_b)$ and similarly for μ_{bc}. The motion of the center of mass is uncoupled from the two other coordinates. For simplicity, we will drop R.

In classical mechanics, the kinetic energy is

$$T = \frac{1}{2}\left(v_a^2 + v_b^2 + v_c^2\right)$$

We now define the Jacobi coordinates suitable to the reactant (A+BC) arrangement. These are the distance between A and the center-of-mass of the BC molecule, and

$$v_1 = u_1 + \frac{m_c}{m_b+m_c}u_2$$

and the BC bond distance

$$v_2 = u_2$$

The relation between the row vector of Cartesian coordinates $\mathbf{q}$ and the row vector of reactant Jacobi coordinates $\mathbf{v}$ is

$$\mathbf{v} = \mathbf{q}\mathbf{T}_{qv} = \mathbf{q}\begin{bmatrix} 1 & 0 \\ \frac{m_c}{m_b+m_c} & 1 \end{bmatrix}$$

or $\mathbf{q} = \mathbf{v}\mathbf{T}_{vq}$ where

$$\mathbf{T}_{vq} = \mathbf{T}_{qv}^{-1} = \begin{bmatrix} 1 & 0 \\ \frac{-m_c}{m_b+m_c} & 1 \end{bmatrix}$$

The relation between the row vector of the gradients **dq** and **dv** is

$$\left[\begin{array}{cc} \frac{d}{dq_1} & \frac{d}{dq_2} \end{array}\right] = \left[\begin{array}{cc} \frac{d}{dv_1} & \frac{d}{dv_2} \end{array}\right] \left[\begin{array}{cc} \frac{dv_1}{dq_1} & \frac{dv_1}{dq_2} \\ \frac{dv_2}{dq_1} & \frac{dv_2}{dq_2} \end{array}\right] = \mathbf{dv}\,\mathbf{T}_{qv}^T$$

Thus, in Jacobi coordinates, the matrix of the kinetic energy operator, analogous to Eq. (139), is

$$\begin{aligned} \hat{\mathbf{T}}_v &= \frac{1}{2}\frac{\mathbf{d}}{\mathbf{dv}}\,\mathbf{T}_{qv}^T\,\mu_q^{-1}\,\mathbf{T}_{qv}\frac{\mathbf{d}}{\mathbf{dv}}^T \\ &= \frac{1}{2}\frac{\mathbf{d}}{\mathbf{dv}}\,\mu_v^{-1}\,\frac{\mathbf{d}}{\mathbf{dv}}^T \end{aligned} \tag{140}$$

where

$$\mu_v = \left[\begin{array}{cc} \mu_{a,bc} & 0 \\ 0 & \mu_{bc} \end{array}\right]$$

Consequently, the matrix of the kinetic energy is diagonal in Jacobi coordinates. We shall make one more simplification, by transforming to *mass-scaled* Jacobi coordinates,

$$S = \lambda^{1/2} v_1$$

and

$$s = \lambda^{-1/2} v_2$$

with

$$\lambda = \left[\frac{\mu_{a,bc}}{\mu_{bc}}\right]^{1/2}$$

Or

$$\mathbf{s} = [S\,s] = [v_1\,v_2]\mathbf{T}_{vs}$$

where

$$\mathbf{T}_{vs} = \left[\begin{array}{cc} \lambda^{1/2} & 0 \\ 0 & \lambda^{-1/2} \end{array}\right]$$

Following the development earlier in this section, leading from the Cartesian to the Jacobi

coordinates, we find

$$\mathbf{dv} = \mathbf{ds}\,\mathbf{T}_{vs}^{T} = \mathbf{ds}\begin{bmatrix} \lambda^{1/2} & 0 \\ 0 & \lambda^{-1/2} \end{bmatrix}$$

so that, in the mass-scaled Jacobi coordinates the matrix of the kinetic energy operator is

$$\hat{\mathbf{T}}_s \frac{1}{2}\frac{\mathbf{d}}{\mathbf{ds}}\,\mathbf{T}_{vs}^{T}\,\mu_v^{-1}\,\mathbf{T}_{vs}\frac{\mathbf{d}}{\mathbf{ds}}^{T} = \frac{1}{2}\frac{\mathbf{d}}{\mathbf{ds}}\,\mu_s^{-1}\,\frac{\mathbf{d}}{\mathbf{ds}}^{T} = \frac{1}{2\mu}\frac{\mathbf{d}}{\mathbf{ds}}\,\mathbf{I}\,\frac{\mathbf{d}}{\mathbf{ds}}^{T} \tag{141}$$

where $\mathbf{I}$ is the unit matrix and μ is the system reduced mass

$$\mu = \left[\frac{m_a m_b m_c}{m_a + m_b + m_c}\right]^{1/2}$$

Thus, in mass-scaled Jacobi coordinates, the matrix of the kinetic energy operator is independent of the choice of the arrangement used to define the Jacobi coordinates.

B. Relation between arrangement Jacobi coordinates

The relation between the mass-scaled Jacobi and the bond coordinates is

$$\mathbf{s}_a = \mathbf{q}\,\mathbf{T}_{qv_a}\,\mathbf{T}_{v_a S_a} = \mathbf{q}\,\mathbf{T}_{qs_a}$$

Here, we have added the subscript a, to designate the arrangement A–BC.

Problem 28

Show that

$$\mathbf{T}_{qs_a} = \left(\frac{\mu_{a,bc}}{\mu_{bc}}\right)^{1/4}\begin{bmatrix} 1 & 0 \\ \mu_{bc}/m_b & (\mu_{bc}/\mu_{a,bc})^{1/2} \end{bmatrix}$$

The relation for the arrangement AB–C is identical, except that the diatomic bond is now q_1. Thus

$$\mathbf{T}_{qs_c} = \left(\frac{\mu_{ab,c}}{\mu_{ab}}\right)^{1/4}\begin{bmatrix} \frac{\mu_{ab}}{m_b} & \left(\frac{\mu_{ab}}{\mu_{ab,c}}\right)^{1/2} \\ 1 & 0 \end{bmatrix}$$

Now, consider the mass-scaled Jacobi coordinates in arrangements a and c. From Eq. (**??**) you can show that

$$\mathbf{s}_c = \mathbf{s}_a \, \mathbf{T}_{qs_a}^{-1} \, \mathbf{T}_{qs_c} = \mathbf{s}_a \mathcal{T}_a$$

where the transformation $\mathcal{T}$ is

$$\mathcal{T}_a = \left[(m_a + m_b)\,(m_b + m_c) \right]^{-1/2} \begin{bmatrix} [m_a m_c]^{1/2} & [m_b M]^{1/2} \\ [m_b M]^{1/2} & -[m_a m_c]^{1/2} \end{bmatrix} \tag{142}$$

Problem 29

Show that the transformation matrix $\mathcal{T}$ is orthogonal, namely $\mathcal{T}\,\mathcal{T}^T = \mathbf{I}$.

As is shown schematically in Fig. 18 the Jacobi coordinates corresponding to the product (AB+C) arrangement $\{R_c, r_c\}$ corresponds to a rotation of the reactant (A+BC) arrangement Jacobi coordinates through an angle Θ followed by a reflection in the R_c axis. This combined transformation is

$$\begin{bmatrix} 1 & 0 \\ 0 & -1 \end{bmatrix} \begin{bmatrix} \cos\Theta & \sin\Theta \\ -\sin\Theta & \cos\Theta \end{bmatrix} = \begin{bmatrix} \cos\Theta & \sin\Theta \\ \sin\Theta & -\cos\Theta \end{bmatrix} \tag{143}$$

Be comparison of this last equation with Eq. (142), we see that the rotation angle, called the *skew* angle, is

$$\Theta = \tan^{-1}\left[\left(\frac{m_b M}{m_a m_c} \right)^{1/2} \right]$$

The skew angle ranges from nearly 0, for a reaction involving exchange of a light atom between two heavy atoms (Cl+HCl→ClH+Cl, for example), to 60^o, for a reaction with equal masses (H+H_2, for example), to 90^o, for a reaction involving exchange of a heavy atom between two light atoms (H+ClH→HCl+H, for example).

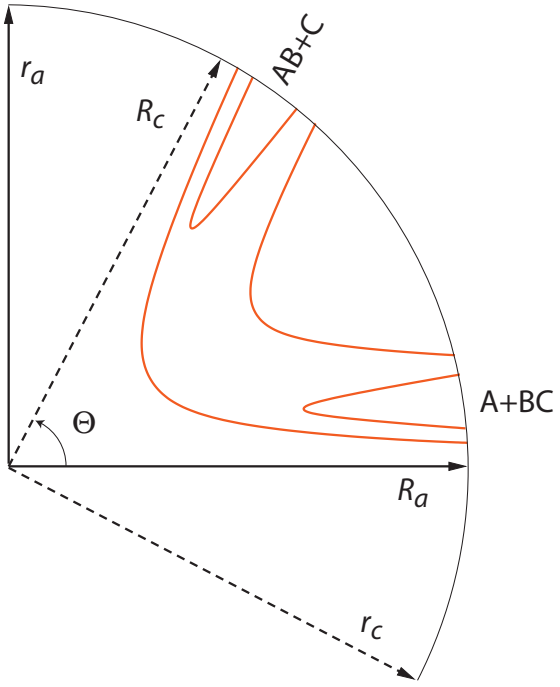

FIG. 18. Reactant (solid) and product (dashed) Jacobi coordinates for a typical reactive system. The two sets of coordinates are related by a rotation through the angle Θ followed by a reflection in the new R_c axis. (Figure taken from Ref. [a]).

[a] D. E. Manolopoulos, "Encylopedia of Computational Chemistry," P. v. R. Schleyer, ed. (Wiley, Chichester, 1998) pp. 2699–2708

VIII. FINITE ELEMENT SOLUTION OF THE SCHROEDINGER EQUATION

A. Generalities

In mass-scaled reactant-arrangement Jacobi coordinates the Schroedinger equation is

$$\left[-\frac{1}{2\mu}\nabla_a^2 + V(S_a, s_a) - E\right]\psi(S_a, s_a) = 0$$

If we premultiply by any arbitrary function (designated a *test function* in the FEM literature) $\phi(S_a, s_a)^*$, and integrate over a domain Ω in the variables S_a and s_a, we obtain

$$\int_\Omega \phi(S_a, s_a)^* \left[-\frac{1}{2\mu}\nabla_a^2 + V(S_a, s_a) - E\right]\psi(S_a, s_a)\, d\Omega = 0$$

Using Green's theorem (integration by parts) and making the further simplification that $\phi(S_a, s_a)$ is real, we can transform this to

$$\int_\Omega \nabla\phi \cdot \nabla\psi \, d\Omega - \int_\Gamma \phi(\vec{n} \cdot \nabla\psi) \, d\Gamma + 2\mu \int_\Omega \phi(V - E)\psi \, d\Omega = 0 \tag{144}$$

Here, $d\Omega = dS_a ds_a$ and we have suppressed the coordinate dependence of the potential. The domain Ω is subtended by the surface Γ; to which $\vec{n}$ is the outward normal. Figure 19 illustrates the boundary (delimited by green lines) for the reactive scattering system shown in Fig. 18.

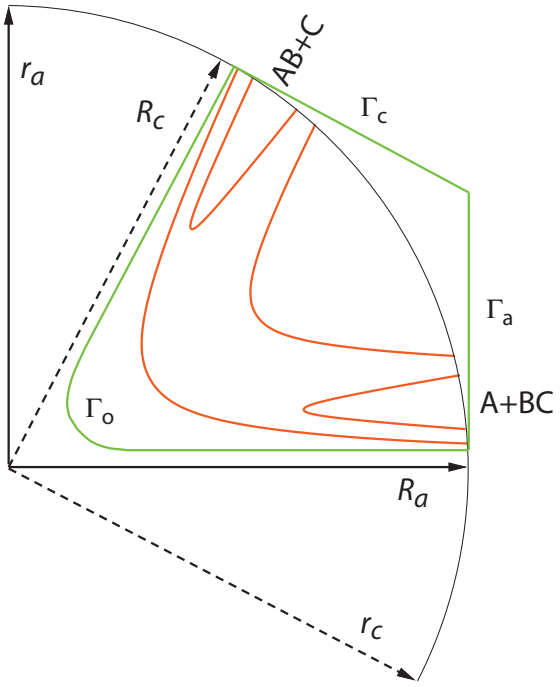

FIG. 19. Illustration of the boundary (drawn in green) of the domain Ω of solution of the Schroedinger equation. The boundary is broken into threes sections: the *outer boundary* along which the scattering wave function vanishes, and the reactant and product boundaries, along which the wave function is described by the usual scattering boundary conditions; see subsection VIII B.

The integrals which appear in Eq. (144) are functionals of two arbitrary functions of the coordinates $u(S_a, s_a)$ and $v(S_a, s_a)$, namely

$$A(u, v) = \int_\Omega \nabla u \cdot \nabla v \, d\Omega$$

(In the FEM literature, this term is called the *bilinear form*), as well as a *boundary integral*

.

$$B(u,v) = \int_\Gamma u(n\cdot\nabla v)\,d\Gamma$$

a *potential matrix*

$$C(u,v) = \int_\Omega uVv\,d\Omega$$

and an *overlap matrix*

$$D(u,v) = \int_\Omega uv\,d\Omega$$

With these definitions, then, the Schroedinger equation becomes

$$A(\phi,\psi) + 2\mu C(\phi,\psi) - 2\mu E D(\phi,\psi) = B(\psi,\phi) \tag{145}$$

We will now triangulate the domain (illustrated also in Fig. 19) by defining n nodes which break up the domain into N triangular elements. We denote by the single coordinate q_i the position of the i^{th} node $\{S_i, s_i\}$. Note that we we use reactant (A+BC) Jacobi coordinates, and will suppress, again for notational simplicity, the subscript a. We expand both the test function and the solution in a set of n functions, denoted ξ_i, which are unity at the i^{th} node and vanish in every triangle which does not include the point q_i as one vertex. Inside this polygonal region these functions are polynomials in S_a and s_a. If these polynomials are restricted to 1^{st} order, the basis functions are irregular pyramids, with the apex located at the point q_i. These 1^{st} order basis functions are designated *hat functions* in the FEM literature, for obvious reason. Expanding gives

$$\psi = \sum_{i=1}^{n} c_i \xi_i \tag{146}$$

Substituting this into Eq. (145), we obtain

$$\sum_{i=1}^{n} \left[A(\phi,\xi_i) + 2\mu C(\phi,\xi_i) - 2\mu E D(\phi,\xi_i)\right] c_i = B(\phi,\psi)$$

Note that we have retained $\psi(q)$ unexpanded in the boundary integral, rather than using the expansion of Eq. (146).

Now, we can replace the arbitrary test function, $\phi(q)$ with any one of the n basis functions.

If, specifically, we chose $\phi(q) = \xi_j$, we obtain

$$\sum_{i=1}^{n} \left[A(\xi_j, \xi_i) + 2\mu C(\xi_j, \xi_i) - 2\mu E D(\xi_j, \xi_i)\right] c_i = B(\xi_j, \psi)$$

Since we have n basis functions, we get a similar equation for each choice of test function with $j = 1 \cdots n$. This implies that we can rewrite the integrated Schrodinger equation in matrix form as

$$\left[\mathbf{A} + 2\mu(\mathbf{C} - E\mathbf{D})\right] \mathbf{c} = \mathbf{b} \tag{147}$$

Here, we use the notation

$$A_{ij} \equiv A(\xi_i, \xi_j) = \int_\Gamma \nabla\xi_i \cdot \nabla\xi_j \, d\Omega$$

and, similarly, for the other matrices. Note that $\mathbf{b}$ is a vector, not a matrix, since we haven't expanded the solution ψ.

B. Boundary integral

As shown in Fig. 19, we define the domain Γ by breaking up the boundary into four pieces: Γ_I, Γ_O, Γ_a, and Γ_c, so that

$$b_i = \int_{\Gamma_I} \xi_i \, (n_I \cdot \psi) \, d\Gamma_I + \int_{\Gamma_O} \xi_i \, (n_O \cdot \psi) \, d\Gamma_O + \int_{\Gamma_a} \xi_i \, (n_a \cdot \psi) \, d\Gamma_a + \int_{\Gamma_c} \xi_i \, (n_c \cdot \psi) \, d\Gamma_c \tag{148}$$

The *inner* Γ_I and *outer* Γ_O delimit regions of high potential energy. Along Γ_I and Γ_O the wave function will be vanishingly small, as will be its derivative footnote explaining this?. Thus, the first two integrals in Eq. (148) will vanish.

At large A–BC separation, the wave function must describe an incoming wave in vibrational state m_0 with outgoing (scattered) waves in all the other energetically accessible vibrational levels, namely

$$\lim_{R_a \to \infty} \psi(R_a, r_a) = \exp(-ik_{m_0} R_a)\chi_{m_0}(r_a) + \sum_{m=0}^{\mathcal{M}} \mathcal{S}^{(a)}_{m_0,m} \exp(ik_m R_a)\chi_m(r_a) \tag{149}$$

Here $\chi_m(r_a)$ is the coordinate-space wave function for the m^{th} vibrational level of the BC fragment with energy ε_m. The wave vector k_m is defined by (in atomic units)

$$k_m = [2\mu_{a,bc}(E - \varepsilon_m)]^{1/2}$$

Finally, the summation in Eq. (149) extends over all $\mathcal{M}+1$ energetically allowed vibrational levels of the BC reactant ($m = 0 \cdots \mathcal{M}$). The quantity $\mathcal{S}^{(a)}_{m_0,m}$ is a matrix element of the *scattering* matrix. The superscript (a) indicates that the individual $\mathcal{S}$-matrix elements refer to initial and final vibrational states in the A+BC arrangement. The absolute value squared of $\mathcal{S}^{(a)}_{m_0,m}$ is the probability of the collisional event A+BC(m_0) $\rightarrow$ A+BC(m).

Along the boundary Γ_a the outward normal is just $\vec{R}_a$, so that

$$n_a \cdot \nabla\psi = \frac{d\psi}{dR_a} = i\left[-k_{m_0}\exp(-ik_{m_0}R_a)\chi_{m_0}(r_a) + \sum_{m=0}^{\mathcal{M}} k_m \mathcal{R}_{m_0,m}\exp(ik_m R_a)\chi_m(r_a)\right]$$

Thus, the contribution of the Γ_a boundary to Eq. (148) is

$$\begin{aligned} b_i^{(\Gamma_a)} &= -ik_{m_0}\exp(-ik_{m_0}R_{ai})\int_{\Gamma_a}\xi_i(R_{ai},r_a)\chi_{m_0}(r_a)dr_a \\ &\quad +i\sum_{m=0}^{\mathcal{M}} k_m \mathcal{S}_{m_0,m}\exp(ik_m R_{ai})\int_{\Gamma_a}\xi_i(R_{ai},r_a)\chi_m(r_a)dr_a \\ &= g_{i,m_0} + \sum_{m=0}^{\mathcal{M}} F_{i,m}\mathcal{S}_{m_0,m} \end{aligned} \tag{150}$$

Here

$$g_{i,m_0} = -ik_{m_0}\exp(-ik_{m_0}R_{ai})\int_{\Gamma_a}\xi_i(R_{ai},r_a)\chi_{m_0}(r_a)dr_a$$

and

$$F_{i,m} = \exp(ik_m R_{ai})\int_{\Gamma_a}\xi_i(R_{ai},r_a)\chi_m(r_a)dr_a$$

Similarly, the contribution of the product boundary Γ_c can be written in terms of a sum over all energetically accessible product vibrational levels $m' = 0 \cdots \mathcal{M}'$ (where the primes designate the AB product vibrational levels) and the component of the $\mathcal{S}$ matrix associated with reactive events, namely

$$b_i^{(\Gamma_c)} = \sum_{m'=0}^{\mathcal{M}'} \mathcal{T}_{m_0,m'}\exp(ik_{m'}R_c)\int_{\Gamma_c}\xi_i(R_{ai},r_a)\chi_{m'}(r_c)dr_c$$

$$= \sum_{m'=0}^{\mathcal{M}'} F_{i,m'} \mathcal{S}^{(c)}_{m_0,m'} \tag{151}$$

I believe that this integral can be evaluated numerically by using Eq. (143) and

$$dr_c = dr_a \frac{dr_c}{dr_a} + dR_a \frac{dr_c}{dR_a} = -\cos\Theta dr_a + \sin\Theta dR_a$$

Formally, then, the boundary vector of Eq. (147) can be written in matrix form as

$$\mathbf{b} = \mathbf{F}\mathbf{s}_{m_0} + \mathbf{g} \tag{152}$$

Here $\mathbf{F}$ is a matrix of N rows (the number of nodes) and N_v columns (the total number of accessible vibrational levels, with $N_v = \mathcal{M} + \mathcal{M}' + 2$); $\mathbf{s}_{m_0}$ is a column vector of the $\mathcal{S}^{(a)}_{m_o,m}$ $\mathcal{S}^{(c)}_{m_o,m'}$ matrix elements and $\mathbf{g}$ is a column vector of length N. Note because the b_i elements all involve integrals over the hat test functions $\xi_i(R_{ai}, r_{ai})$, the elements of both the $\mathbf{b}$ and $\mathbf{g}$ vectors will vanish except when the index i corresponds to a node located along the Γ_a and Γ_c boundaries.

We can now combine Eqs. (147) and (152) as

$$[\mathbf{G}\,\mathbf{F}]\,\mathbf{d} = \mathbf{g} \tag{153}$$

where $\mathbf{G}$ is an $n \times n$ matrix, $\mathbf{F}$ is an $n \times n_v$ matrix, $\mathbf{d}$ and $\mathbf{g}$ are $(n + n_v) \times 1$ column vectors. The first n elements of the $\mathbf{g}$ vector are the expansion coefficients of Eq. (146). The $(n+1)^{st} - (n+n_v)^{th}$ elements of the $\mathbf{d}$ vector are the reflection or transmission coefficients s_{m0}. The matrix $\mathbf{F}$ and the vector $\mathbf{g}$ are zero except for rows corresponding to nodes lying along the Γ_a and Γ_c boundaries. Solution of this set of linear equations [Eq. (153)] will yield the scattering wave function as well as the reflection and transmission coefficients.

Unfortunately, this set of equations is underdetermined, since the solution vector $\mathbf{d}$ has more elements than the number of nodes. We can eliminate this deficiency by taking into account the fact that the wave function along the boundaries Γ_a and Γ_c is doubly defined by Eqs. (146) and (149). In other words, for each value of the index i corresponding to a node lying on the Γ_a or Γ_c boundaries, we have

$$\psi(R_{ai}, r_{ai}) = c_i = \exp(-ik_{m_0} R_{ai})\chi_m(r_{ai}) + \sum_{m=0}^{\mathcal{M}} \mathcal{R}_{m_0,m} \exp(ik_m R_{ai})\chi_m(r_{ai}) \tag{154}$$

or, in matrix notation

$$\mathbf{c} = \mathbf{h} + \mathbf{P}\mathbf{s}_{m_0}$$

Let n_b be the number of nodes lying on the Γ_a and Γ_c boundaries. Then, the column vectors $\mathbf{c}$ and $\mathbf{h}$ have n_b rows, and the matrix $\mathbf{P}$ is dimensioned $n_b \times n_v$.

We can combine this with Eq. (153) as follows:

$$\left[\begin{array}{c|c} \mathbf{G} & \mathbf{F} \\ \hline \mathcal{I} & -\mathbf{P} \end{array}\right] \left[\begin{array}{c} \mathbf{c} \\ \hline \mathbf{s} \end{array}\right] = \left[\begin{array}{c} \mathbf{g} \\ \hline \mathbf{h} \end{array}\right]$$

Here $\mathcal{I}$ is a matrix of dimensions $n_b \times n$ with elements

$$\mathcal{I}_{ij} = \delta_{ij}$$

If $n_b > n_v$, this system of linear equations is overdetermined. However, the additional equations reflect a linear dependency, because the coefficients of the large number of hat functions along the Γ_a and Γ_c boundaries are constrained to be a linear combination of a smaller number of vibrational functions multiplied by incoming or outgoing waves. Solution will yield both the scattering wave function as well as the reactive transmission and inelastic reflection coefficients, subject to this linear dependency.

IX. EVALUATION OF THE MATRICES

A given triangle Consider a triangle formed by the vertices q_i, q_j, and q_k. In the 1^{st} order limit, within this triangle the basis function $\xi_i(S_a, s_a)$ can be written as

$$\xi_i(S_a, s_a) = a_{i;jk} S_a + b_{i;jk} s_a + c_{i;jk}$$

[1] J. M. Blatt, J. Comput. Phys., **1**, 382 (1967); M. S. Child, *Molecular Collision Theory*, 2nd ed. (Academic, New York, 1974); http://en.wikipedia.org/wiki/Numerov%27s_method.

[2] E. W. McDaniel, J. B. A. Mitchell, and M. E. Rudd, *Atomic Collisions: Heavy Particle Projectiles*, (Wiley-Interscience, 1995).

[3] H. Goldstein, *Classical mechanics*, (Cambridge, Addison-Wesley, 1951). This book is now in the third edition and remains a classic.

[4] Http://integrals.wolfram.com/index.jsp.

[5] At large r the integrand behaves as $r^{-3/2}$ which integrates to $1/\sqrt{r}$, which goes to zero very, very slowly.

[6] Http://en.wikipedia.org/wiki/Double-slit_experiment.

[7] M. Abramowitz and I. Stegun, Natl. Bur. Stand. Appl. Math. Ser. (1965), Vol. 55, Chapter 10; see http://www.iopb.res.in/∼somen/abramowitz_and_stegun/intro.htm#00; http://wapedia.mobi/en/Bessel_function.

[8] Http://en.wikipedia.org/wiki/List_of_integrals_of_irrational_functions.

[9] The presence of the k in the denominator ensures that both terms on the right hand side of Eq. (60) will be dimensionless. The scattering amplitude, as we have defined it, is dimensionless. Most often, you see Eq. (60) without the k in the denominator, in which case the scattering amplitude has dimensions of length.

[10] Equation (74) differs from many statements of the optical theorem (see, for example, http://en.wikipedia.org/wiki/Optical_theorem) by the presence of an additional factor of k in the denominator. This is because we have chosen the scattering amplitude to be dimensionless. Many authors do not include the factor of k in the denominator of the 2^{nd} term in Eq. (60), in which case their scattering amplitude is equal to our definition divided by k.

[11] F. D. Colavecchia, F. Mrugała, G. A. Parker, and R. T Pack, J. Chem. Phys. **118**, 10387 (2003).

[12] B. R. Johnson, J. Chem. Phys. **69**, 4678 (1978).

[13] J. M. Blatt, J. Comput. Phys. **I**, 382 (1967).

[14] K. Smith, *The Calculation of Atomic Collision Processes*, Wiley-Interscience, New York, 1971.

[15] A. E. Thorlacius and E. D. Cooper, J. Comp. Phys. **72**, 70 (1987). Note that on page 73, these authors recommend using the new propagator only beyond the classical turning point, in other words, only when $\tilde{T}_{nn}$ is negative.